GEM TN-93-439
PITT/GEM 93-2

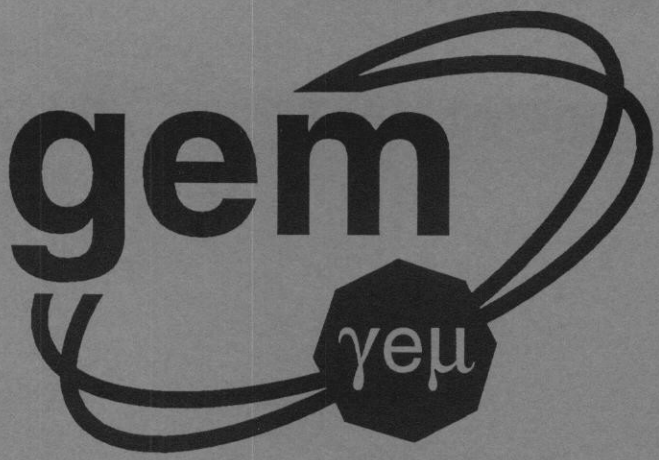

Detailed Studies of the Level 1 Calorimeter Trigger for Higgs $\rightarrow 2\gamma$

Mark Clemen and Bill Cleland
University of Pittsburgh
Department of Physics and Astronomy

July 12, 1993

Abstract;

The performance of the GEM first level single-photon calorimetry trigger is investigated for several sets of trigger criteria. The use of 8 neighboring EM sums for the lateral isolation veto is preferred over the 8 neighboring SPEM sums. Isolated shower recognition is complicated by shower spreading over 2 and more EM sums, leading to trigger inefficiencies by incomplete energy containment near threshold, and self-vetoing by shower spreading beyond threshold. A loosened isolation veto is preferred for single EM sums over threshold. Timing requirements with the new rack layout force the creation of trigger "towns", which are groups of lateral isolation neighborhoods(1.25 x 1.25) in (η x ϕ); trigger performance is changed very little.

PITT/GEM 93-2
July 12, 1993

Detailed Studies of the Level 1 Calorimeter Trigger for Higgs $\rightarrow 2\gamma$

Mark Clemen and Bill Cleland
University of Pittsburgh
Department of Physics and Astronomy

July 12, 1993

Abstract

The performance of the GEM first level single-photon calorimetry trigger is investigated for several sets of trigger criteria. The use of 8 neighboring EM sums for the lateral isolation veto is preferred over the 8 neighboring SPEM sums. Isolated shower recognition is complicated by shower spreading over 2 and more EM sums, leading to trigger inefficiencies by incomplete energy containment near threshold, and self-vetoing by shower spreading beyond threshold. A loosened isolation veto is preferred for single EM sums over threshold. Timing requirements with the new rack layout force the creation of trigger 'towns', which are groups of lateral isolation neighborhoods (1.25 x 1.25) in (η x ϕ); trigger performance is changed very little.

1 Introduction

An important part of the 1st level calorimeter triggering is the single photon trigger. The discovery of new exchange bosons and the study of new physics both rely on the single photon trigger. This trigger should indicate the location of any isolated Electromagnetic (EM) showers present over several thresholds for further trigger processing. The intrinsic efficiency and inherent biases of this trigger will directly impact the capability of the GEM experiment.

The hardware implications of this trigger are no less important. The grouping of calorimeter towers into trigger sums, the information to be made available to the trigger electronics, and the type and amount of information exchanged between trigger racks are all largely driven by the single photon trigger. These considerations have further ramifications on system speed and cost.

The number of trigger sums directly affects the cost. The pressure within the collaboration to minimize system costs had direct effects on the trigger configuration originally proposed. The information passed between trigger sums determines the large-scale cabling, which in turn affects the system latency. The scope of the calorimeter information necessary to make a reliable trigger decision determines the overall complexity of the trigger hardware; simplicity leads to lower cost and higher system reliability. These considerations have led us to investigate the problem of the single photon trigger further.

2 Baseline SP Sum Lateral-Vetoing

The baseline trigger algorithm is shown in Figure 1. The smallest segmentation in the EM section are the EM sums. All sums are sums of transverse momentum (Pt) from the weighted energy in each calorimeter tower. All energy thresholds referred to here are thresholds on these weighted-energy Pt sums. In the barrel, the EM sums are non-overlapping sums of 6x6 towers, which are (.157, .157) in (η, ϕ). The EM sums themselves are summed together 2x2 to form the SPEM sums of (.314, .314) in (η, ϕ). The first floor of the hadronic section also has its towers summed to form (.314, .314) sized energy sums in (η, ϕ), such that these overlap the SPEM sums.

The baseline trigger forms two logical quantities. The trigger is satisfied if the logical 'OR' of these two quantities, with the hadronic veto requirement, is true.

```
EMV1:
        (central SPEM greater than Pt threshold)
.and.   (3rd largest EM sum within the central SPEM sum
            is less than 1 GeV)
.and.   (largest SPEM neighbor is less than 1 GeV)
.and.   (central EM sum in the central SPEM sum is larger
            than the other EM sums in the central SPEM sum)

EMV2:
        (central EM sum is greater than 2/3 threshold)
.and.   (largest SPEM neighbor is over 1/3 threshold)
.and.   (2nd largest EM sum within the central SPEM sum is
            less than 1 GeV)
.and.   (central SPEM sum is greater than any SPEM neighbor)
.and.   (2nd largest SPEM neighbor is less than 1 GeV).
```

The first condition is designed to trigger on showers that are spread between two EM sums within an SPEM sum, and the second those showers that spread between two EM sums in adjacent SPEM sums. In addition, the nearest 4 SP1 hadronic sums behind the central EM sum are all required to be less than 5 GeV.

This 'standard trigger' was modelled using QFL, the CDF shower parameterization code which employs the Boch parameterization. Events were generated (without bunch-crossing related pileup) using ISAJET. For efficiency studies, 80 GeV Higgs and 140 GeV top events were also generated using ISAJET. Table 1 summarizes the data set. In the interest of speed and simplicity, a spherical calorimeter was simulated. Figure 2 shows a comparison in background rates between this simulation and the same trigger configuration coded in GEMFAST. GEMFAST uses a cylindrical barrel calorimeter

File Type	Pt Range (GeV)	Cross Section (mb)	Events
2-Jet	10 - 20	14.93	5000
2-Jet	20 - 40	2.198	5000
2-Jet	40 - 80	.2542	5000
2-Jet	80 - 160	.02500	2500
2-Jet	160 - 320	.001964	2500
QED Photon	10 - 20	.00111	1000
QED Photon	20 - 40	.0002354	1000
140 GeV Top	100 - 200		2500
80 GeV Higgs	1 - 1000	gam-gam	5000

Table 1: ISAJET Monte Carlo Data Set Summary

and a different shower parameterization. The results are comparable. What is not shown is that QFL runs 15 times faster. For analysis simulation or detector studies, one would probably not use QFL. Since we are grouping the calorimeter response into bins coarser than an energy shower radius, we judged QFL to be a good measure of the trigger rates and efficiencies for the configurations discussed here.

There are other reasons beyond trigger rates and efficiencies for doing these studies now. The choice of the (.157, .157) segmentation has been called into question by those considering system costs. A coarser segmentation in the barrel would lead to fewer channels, which would lower the cost of the first level trigger. Therefore, we have pursued our trigger studies here for many segmentations. Since the topology of high energy collisions at SSC energies is not currently known, the conservative approach would seem to be to pick a smaller EM segmentation consistant with shower containment. However, it is concievable that there is some optimum segmentation, not (.157, .157), that gives the best photon efficiency for a given trigger rate.

Figure 3 shows the background single photon trigger rates as a function of

energy threshold for the above trigger criteria at the standard SSC luminosity. For this simulation the EM sums were made exactly (.157, .157), for all regions from η in (-2.8, 2.8). There is no gap or material included between the barrel and the endcaps. Interestingly enough the highest background trigger rate at the lowest threshold is exactly at the nominal trigger segmentation of (.157, .157). At higher thresholds, larger segmentations dominate. There is an interesting tradeoff implicit in this graph, between the increasing ability to concentrate energy in a single bin with larger segmentations, and the higher probability to veto the "isolated shower" as the lateral veto region increases. (All sums scale here: the SPEM and SP1 sums are all twice the EM sum size). As the EM sum size increases, a larger and larger swath of calorimetry is defined as the veto region, with the same requirement of less than 1 GeV energy deposit being made within this region.

Figure 4 shows the efficiency for detecting an 80 GeV Higgs decaying to 2 gammas, where one or both falls within the trigger acceptance. This peaks for the nominal (.157, .157) segmentation, clearly because the larger lateral veto area cuts into the efficiency through accidental overlap. The top quark efficiency is inherently different. Top quark decays will have associated particles near to the EM shower, so that the signal tends to veto itself. Figure 5 shows that the efficiency for top is best when the lateral veto region is the smallest.

Our goal though is to accumulate the Higgs $\rightarrow 2\gamma$ signal as best as can be done, without accepting too many background triggers. Figure 6 shows the Higgs efficiency against the trigger rate, for the different segmentations. Each point is taken at one of the previously shown thresholds. The highest trigger-rate point corresponds to 15 GeV Pt threshold, the next to 20 GeV, etcetera, for each segmentation. The (.157, .157) segmentation is near ideal. The (.105, .105) case is similiar, but would cost more, while the (.209, .209) case gives somewhat less Higgs efficiency for the same trigger rate. Presumably this is caused by the larger lateral veto region, allowing low energy particles in the same event to accidently veto an otherwise isolated photon. The (.157, .157) segmentation seems optimal for the baseline photon trigger.

The efficiency for capturing a low-mass Higgs is one of the primary goals in the GEM experiment, but the efficiency for triggering on a single photon is what one is most interested in. Assuming the (.157, .157) segmentation at a 15 GeV threshold, the Higgs single-photon efficiency is shown as a function of η in Figure 7. This efficiency is found by asking whether a particular EM

sum triggered, when a photon from Higgs decay above some threshold passed through its fiducial area. Somewhat surprisingly, this efficiency is flat out to the limit here of $|\eta|$=2.8. At high η, the (.157, .157) geometry begins to make the trigger sums somewhat smaller than a shower diameter; one might have expected a decrease in efficiency, which is not evident. This trigger algorithm though is largely based on the SPEM sums, so perhaps this is not so surprising. Another interesting feature is the magnitude. The photon efficiency averages to only 77 % here.

Figure 8 shows the background trigger rate as a function of rapidity. Events were double-binned for statistics. Once again, the trigger sums in this simulation are precisely (.157, .157), out to the highest η. There is no gap here between the barrel and the endcap, contrary to what may seem indicated. The fluctuations are still large, but the background rate seems flat over the full trigger region.

3 EM Sum Lateral Vetoing

There have been several worries with the baseline trigger. One is that the noise in an SPEM sum is near to 1/2 GeV, so that the 1 GeV lateral veto threshold is only 2 sigma above the noise. Another possible objection is that the lateral veto region is large in (η, ϕ) space, covering a "doughnut" that is (.942, .942) across. Aside from issues of accidental overlap between a jet and an otherwise bona fide isolated photon, this may create a bias for some physics. This would be true of a top quark photon trigger, where some associated EM energy is expected nearby. Perhaps some other, currently unforeseen physics signal, would suffer likewise. Such a bias would be aggravated in the endcaps, where the EM sums are foreseen to be larger than the nominal (.157, .157).

In an attempt to choose a set of trigger criteria that might mitigate some of the above problems, we tried one that would narrow the lateral veto region. In this scheme, the 8 EM neighbors are used, rather than the 8 SPEM neighbors. Previous work when the trigger ideas were being developed had indicated that the background trigger rate with this algorithm would be too high; this was resurrected to see what might be done. The trigger conditions here are:

```
EMV1:
      (central EM sum is greater than threshold)
.and. (1st largest EM neighbor is less than 1 GeV)

EMV2:
      (central EM sum is greater than 2/3 threshold)
.and. (1st largest EM neighbor is over 1/3 threshold)
.and. (2nd largest EM neighbor is less than 1 GeV)
```

The hadronic veto was also changed from the 4 SP1 sums behind the central EM sum to just the one SP1 sum. This alone was required to be less than 5 GeV. Figure 9 shows a comparison of the Higgs efficiencies versus background rates for this longitudinal-veto region and a larger one covering 4 SP1 sums. Also shown is the Baseline SP Sum photon trigger. One sees that the points for the EM Sum lateral vetoing with 1 hadronic SP sum vetoing are almost indistinguishable from those with 4 hadronic sums vetoing. For the same Higgs efficiency, the background rate is marginally smaller for the latter. Surprisingly, there is little difference between the baseline SP-vetoing and the EM-vetoing proposed here. The baseline trigger has a somewhat flatter slope, presumably caused by accidental vetoes in the larger veto region. One might even conjecture about the universality of this curve, for broadly similar trigger conditions.

Figure 10 shows the background trigger rates for this new set of criteria (EM sum veto), as a function of energy threshold. Now it is the (.209, .209) segmentations and larger that give the highest background rates. Note that the (.157, .157) rates have changed very little. This trigger is also less biased against event related overlap, and therefore the efficiencies will be less dependent on event topology with this trigger. This is a benefit here, since the results are less dependent on the details of the Monte Carlo.

Figure 11 shows the 80 GeV Higgs efficiency for the different segmentations. The segmentation that gave the higher trigger rates also gives the best efficiency for the Higgs $\rightarrow 2\gamma$. Again, this indicates that one is maximizing the energy in one EM sum while minimizing the lateral accidental overlap. We are interested in getting the best Higgs efficiency for the same trigger rate, and in Figure 12 one sees that this function has very little dependence on the segmentation as one might have previously thought. For this set of

trigger criteria it is not clear that the (.157, .157) trigger segmentation is optimal. While the background rate goes up for some segmentations, so does the efficiency, and as is seen in Fig. 9, the points seem to lie on a common curve of efficiency vs. rate. At the lowest energy thresholds (highest trigger rates) one sees that the (.105, .105) case falls below the curve, presumably because the segmentation is becoming smaller than a shower diameter, and that the (.314, .314) case also may fall a bit low. At intermediate energy thresholds (intermediate trigger rates) the (.157, .157) and (.209, .209) segmentations maintain their efficiencies well for a given trigger rate, though they do fall off a bit at higher energy thresholds (lower trigger rates). Even if not currently optimal, the functional dependence on the trigger sum size is weak.

Finally Figure 13 shows the top efficiency versus the trigger threshold. Since we no longer veto on such a large lateral region, the order of the segmentations that give the best efficiency changes very little until the (.262, .262) size is reached (lateral veto area of (.786, .786)). Figure 14 shows the top efficiency against the background trigger rate, again showing that the smaller 3 segmentations are best. These are included for the reader's interest; the top efficiency is not a driving consideration in the trigger segmentation at the SSC.

4 Two Ring Lateral Vetoing

A lateral veto on the isolated photon shower that uses more information would be the previous set of criteria, using the 8 neighboring EM sums (7 when the shower is allowed to spread over 2 sums), and then further using the 16 EM sums surrounding those. This two-ring trigger would be difficult to implement, but has been explored before in an attempt to suppress background trigger rates further. The lateral vetoing area would be similar to the SP-Sum lateral vetoing, but with more information used. Figure 15 shows the Higgs efficiencies versus the background trigger rates with and without this second ring. While the 1-ring lateral veto gives higher background trigger rates for the same energy threshold, one sees that the two sets of points lie on the same line. One does not get any more efficiency for the Higgs at a given background trigger rate with the two lateral rings.

5 Trigger Efficiency Magnitudes

The trigger efficiencies that have been shown so far are less than 100%, even 90%. We undertook a study to understand what events were being lost and how. Figure 16 shows an example trigger response curve to single photons in different energy bins. These were taken from the 80 GeV Higgs boson events and from the direct photon data sets, at a trigger threshold of 25 GeV. One sees a nice step at the trigger threshold, with a shoulder at the trigger threshold, and a final rise to the full efficiency.

There are two questions.

- Why is the efficiency only 70% or so near threshold?
- Why doesn't the efficiency rise to a full 100%?

Figure 17 shows scatterplots of the shower sharing for the Higgs photon events near threshold. For both plots there is a hadronic veto cut, and a lateral isolation cut on the 2nd outside ring of EM sums. There are no lateral isolation cuts in the immediate neighborhood of the center EM sum. There is an energy cut. At each trigger threshold, the total energy in a 9x9 array of EM trigger sums was summed. When this total was greater than the trigger threshold, but not greater by more than 5 GeV, with the central EM sum contributing more than its neighbors, then the shower was enterred into this scatterplot. The horizontal scale is the central EM-sum divided by the trigger threshold energy. The vertical scale is the highest EM sum neighbor, of the 8 neighbors that the central sum can have. This is also normalized to the trigger threshold. The underflows are those entries where the highest immediate neighbor is less than 1 GeV.

The shower sharing between the central EM sum and the highest neighbor is clear here. There is a smeared line beginning at no sharing (all of the energy in the central tower, and none in the highest neighbor), going linearly through the possible sharings. (10%/90%, 20/80, etc.). The figure on the left has no lateral isolation cut, the figure on the right requires 7 of the 8 neighbors be less than 1 GeV. Qualitatively one sees the effect of the lateral isolation cut - those with shower sharing giving a significant amount of energy in a 3rd EM sum get cut.

The EM trigger is easily represented in this plot. The isolated EM sum trigger requires more than the threshold energy in the central EM sum, and

requires that the highest neighbor be less than 1 GeV. The first (underflow) bin on the vertical axis represents this cut; events appearing in the scatterplots proper have more than 1 GeV in the highest neighbor, sufficient to satisfy the veto in the EMV1 trigger. In the scatterplot on the left, 53.4% of the showers have more than the threshold energy. Both EMV1 criteria together include the entries in the scatterplot to the right of the vertical solid line and below the horizontal solid line; this represents 50.3% of the total EM showers shown. (An energy deposit of less than 5 GeV in the hadronic section is also required). The EMV2 sum sharing trigger requires more than 2/3 of the threshold energy in the central EM sum, and more than 1/3 in the highest neighbor. This would include the entries above the intersection of the two dashed lines in the plot, and represents 8.5% of the total. Without any lateral veto requirements, this trigger accepts (50.3 + 3.1 + 8.5) = 61.9% of the showers within 5 GeV of threshold.

The trigger allows shower sharing only between 2 EM sums. The left scatterplot contains showers that are spread over 2, 3 and 4 EM sums. There is no restriction on the lateral shower spreading about the central EM sum, save that on the outside ring of the 5x5 matrix. This should be small, since we are only considering photons near threshold. The scatterplot on the right in Figure 17 has a cut on the inside 3x3 matrix, requiring the other 7 neighbors to be below 1 GeV, reducing the problem to shower sharing between 2 EM sums.

With the isolation cut alone on the 7 neighbors, 6% of the entries in the plot are lost, from the region where the discriminator trigger is not being applied. For photons near threshold then, 3- and 4-EM sum sharing is negligible. One could change the 2/3 - 1/3 sharing criteria to 70/30, but the dashed line on the left would rise and cut more events as the dashed line on top was lowered and included more events. Thus the loss (area of the box) is decreased, but so is the efficiency. There seems little room for optimisation. With the EMV1 and EMV2 lateral isolation cuts, the scatterplot on the right shows that the trigger accepts (50.3 + 8.3) = 58.8% of the showers near threshold.

This then answers the first question above. The initial rise in the discriminator curve is dependent on the EM sum shower sharing conditions, which are important for photons near the threshold energy. The second question remains open. We suspected that the reason that the discriminator curve does not rise to a full 100% efficiency is that the sharing to other EM sums

violates the 1 GeV lateral veto threshold.

To investigate this, we formed the same scatterplots as in Figure 17, but for photons 10-15 GeV over threshold. See Figure 18. Again, the scatterplot on the right requires the 7 EM neighbors to be less than 1 GeV, and the scales are normalized to the trigger threshold. The lateral isolation requirement cuts 7% of the showers between the two scatterplots. The two trigger criteria include 76.9% of the showers including the isolation cut, that is, the sum of the region below the two solid lines and the 2 regions above and to the right of the dashed lines. It is easy to see that including all showers over threshold with no requirement on the EMV1 highest neighbor would include another 15%, for a total of 92% of the showers, a very good efficiency.

We then changed the shower sharing part of the trigger, so that the 2nd highest neighbor was not required to be less than 1 GeV, but was rather left unconstrained. The 3rd highest neighbor was required to be less than 1 GeV. Specifically, the EMV2 condition defined above was changed to be :

```
EMV2:
      (central EM sum is greater than 2/3 threshold)   .AND.
      (largest EM neighbor is over 1/3 threshold)      .AND.
      (3rd largest EM neighbor is less than 1 GeV)
```

This left one unconstrained neighbor. We also did a seperate run, leaving 2 unconstrained neighbors.

```
EMV2:
      (central EM sum is greater than 2/3 threshold)   .AND.
      (largest EM neighbor is over 1/3 threshold)      .AND.
      (4th largest EM neighbor is less than 1 GeV)
```

Note that there is no spatial requirement on the position of the neighbor.

The results are shown in Figure 19. While the efficiency does improve above threshold, it still does not go to 100%, except maybe for the highest photon energy point in the second case. Leaving just one unconstrained neighbor hardly changes the curve at all. One concludes that once there is a shower that spreads to two EM trigger sums, that there is little significant spreading to more.

The trigger has two parts though. In addition to the above, we further loosened the lateral veto criteria on EMV1, the isolated EM sum part of the trigger. First we allowed the highest neighbor to be unconstrained while the central was still above threshold, and then allowed two neighbors to be unconstrained. The others were still required to be less than 1 GeV. The discriminator curves for this case are shown in Figure 20. For photons near threshold, the efficiency goes up somewhat for both cases where the lateral veto constraint is lessened. More importantly, when there are two neighbors left unconstrained, the efficiency goes to the 100% for high enough photon energy beyond threshold.

One also sees in this plot that when 1 neighbor is left unconstrained, the efficiency initially rises to near 100%, then falls again. As the shower energy increases, spreading to more than 1 nearby EM sum becomes important enough to significantly affect the efficiency. Figure 21 shows this same case for the (.209, .209) segmentation. Since lateral shower spreading is less for the larger EM sums, one sees less sign of it in the plateau of these curves.

By refering back to the same plot of efficiency versus rate, one may get an idea of whether this is worth considering further. Figure 22 shows the nominal trigger compared to three cases of loosening the lateral veto constraints. One leaves two neighbors unconstrained in only the isolated sum trigger EMV1, one in only the 2-sum sharing EMV2, and the third leaves two neighbors unconstrained in both triggers EMV1 and EMV2. Only in the cases where the EMV1 trigger is loosened does one depart from the nominal curve at all, and even then not by very much. Figure 23 shows that all of the benefit actually comes when leaving just 1 neighbor unconstrained in the EMV1 trigger.

We conclude from this then that while we observe a shoulder in the efficiency as the photon energy is increased beyond the trigger threshold, and that the eventual efficiency is less than 100%, that there is little to be done about it. The first is inherent in 2-sum sharing algorithms, and the second is due to shower spreading when an otherwise isolated EM sum is well over threshold. Larger sums can mitigate the lateral shower spreading, but we have seen in Figure 12 that for a given trigger rate, that the Higgs efficiency does not rise significantly for the larger segmentation with the larger corresponding veto region.

That the improvement in efficiency at a given trigger rate is only a modest one is interesting. The changes in the trigger criteria that were applied to

the isolated photons were also applied to the background. That the efficiency changes little with rate indicates not that the background is staying the same. It indicates something about the character of the background, possibly narrower neutral jets, that have a exponentially decreasing (or increasing) change in rates as cuts are applied that affect the actual isolated photons linearly against the same parameter. Even a trigger that is based on the floating point addition of energy deposits about the triggering EM sum would be fooled by lateral spreading that makes an otherwise isolated photon look more like the neutral jet background. Any improvements that can be made on the nominal EM-veto trigger presented here would be modest at best.

6 Other Trigger Dependences

Since shower spreading beyond the central EM sum is hurting the overall trigger efficiency to some degree, we investigated raising the threshold on the nearby neighbors. This threshold has been 1 GeV. It could be as low as 700 MeV, and still be 3 sigma above the noise. It can be as high as one likes. Figure 24 shows the Higgs efficiency versus the trigger rate for several lateral veto thresholds in this range. While one moves along the previously defined curve, there is no benefit from changing the lateral threshold in actual Higgs efficiency for a given trigger rate. Figure 24b shows the effect of changing the lateral veto on the trigger turn-on curve, for a 15 GeV trigger threshold. The photons near threshold are perhaps effected, but those well over are not, by small changes in the lateral veto level.

This curve of efficiency versus background rates is more interesting the less that it changes. There seems to be little that can be done to deviate very far from the norm. Of course, the cuts so far have been on energy thresholds of nearby neighbors. Perhaps by implementing a simple pattern recognition beyond the shower isolation, one would introduce further information that would change the position of the efficiency versus rates curve.

In leaving 2 EM sum neighbors unconstrained in the previous section, they were chosen by energy ordering in the list of all neighbors. Instead of ordering them in this fashion, we chose them so that in the case of 2-sum shower sharing, the neighbor to the left and to the right of the primary sharing neighbor are those left unconstrained. There is no obvious way to choose them in the isolated EM sum case, so that the EMV1 isolation part

of the trigger was left unchanged from the nominal trigger. The results are shown in Figure 25. Again, there is no deviation from the standard efficiency versus rate curve. In retrospect, this is not so surprising, since we have already shown that when the shower spreads significantly between 2 EM sums, that there is little shower spreading beyond that.

If one believes that the background is principally due to unusually narrow jets with unusually large EM energy components, then it is possible that since lateral cuts have failed to make any headway against this that changing the longitudinal cuts may. There may still be some fraction of hadronic energy that would make the background sensitive to the hadronic cuts. Figure 26 shows that efficiency versus background for several different hadronic cuts. It is true that the Higgs efficiency doesn't change at all, while the trigger rate does. The pileup and thermal noise in the front-floor hadronic SP sums totals 1.1 GeV at a luminosity of 10**33. The veto threshold would be at least 3 sigma above the noise. The actual benefit in Higgs efficiency against background is seen to be slight for a wide range of thresholds. Further pattern recognition seems unlikely with the (.157, .157) EM sum size, in a way that would allow one to significantly change the efficiency versus rate curve.

7 Rapidity Dependences

The discussion of the trigger simulation has only been for bins of equal (η, ϕ) over the rapidity range of (-2.8, 2.8). The actual configuration of EM trigger sums will look more like those shown in Figure 27 in the endcaps. Without getting into simulating particular configurations, one would like to argue about the global aspects of larger trigger sums or larger lateral veto areas versus rapidity.

Figure 28 for instance shows the single photon efficiency as a function of rapidity for the (.157, .157) segmentation at a trigger threshold of 15 GeV. For simplicity we will use the trigger threshold of 15 GeV for all of the comparisons here. One also sees that the efficiency is fairly flat, with perhaps some falloff at the highest η near the trigger limit foreseen ($\mid \eta \mid = 2.5$).

As one goes towards higher rapidities the EM trigger sum should get larger, to contain the EM shower if for no other reason. Figure 27 shows EM sums no smaller than 4 Moliere radii across. Also, those sums at the limit of the endcap trigger region would be used for lateral vetoes only for shower

isolation testing. These can be narrower in η, and wider in ϕ.

Figures 29 and 30 show the Higgs photon efficiency for two larger EM sum sizes. Both are flat up to the expected trigger limit of 2.5=$\mid \eta \mid$. One might not expect that a conglomeration of the 3 will also be flat in η, since they are flat at different levels. This is true even when the lateral veto region is changed while keeping the EM sum size the same. Compare Figures 15 and 7, showing the EM and SP lateral vetoing for the (.157, .157) segmentation. There is no inherent flaw in the trigger scheme that obviates certain rapidity regions from otherwise equal consideration.

One other worry would be that there are some regions of rapidity that contribute more to the background trigger rates. One might suspect for instance that it is the forward rapidities that are disproportionally represented in the background rates in spite of the proportional (η, ϕ) lateral veto regions. Figures 31 - 33 show the background trigger rates for different trigger sum sizes. The lateral veto areas scale accordingly. The effects of these different sum sizes are convoluted, but none show a significant change in trigger rate in the trigger region up to $\mid \eta \mid$=2.5 (Some show a change in rate beyond that.) Figure 8 shows the background rates versus rapidity for the SP lateral vetoing, which when compared to Figure 31 shows the effect of keeping the EM sum size the same but changing the lateral veto region. Again, there is no strong dependence on η in the trigger region. Note also Figures 32 and 33. There is no gap between the barrel region and the endcap region, as might seem to be indicated. By showing that things do not inherently change in the endcaps for different EM sum sizes and for different lateral veto regions, we can conclude that there will be no significant biases in changing the EM sum sizes and lateral veto region sizes near the rapidity limit of the trigger.

8 Preamplifier Gain Dependences

Figures 34 and 35 show the discriminator curves for the 15 GeV and 25 GeV thresholds as inter-channel preamp gain discrepancies are introduced between the towers going into the EM sums. This also includes the towers going into the hadronic SP sums. The gain differences were assumed to fall on a Gaussian, with a sigma as shown. Here the Higgs photons were combined with the direct QED photon data sets to increase the statistics in each photon energy bin. One sees that the photons immediately below

threshold and those just above threshold are most affected. The sharp edge on the discriminator curve becomes more gradual. It is expected that, with the large numbers of preamplifiers produced, it will be possible to group them in batches with the dispersion in relative gains of less than 5%. Even at 5% one sees that the discriminator curve is only mildly affected. Smaller gain deviations showed no difference from the nominal within statistics. Given the difficulties that the 2 EM-sum shower sharing algorithm has near threshold already, this trigger is not sensitive to calorimeter channel-to-channel gain problems.

9 Physical Layout

The 1st level trigger was originally foreseen as being located above the calorimetry, arranged in a circle. This minimizes the path lengths of the interconnects required to pass the lateral veto information between racks of EM sums. The trigger now is located on the wall of the experimental hall, arranged in a plane. The length of the interconnects now poses a problem for the timing. It is difficult to see how the 2 microsecond latency can still be achieved.

One suggestion has been to eliminate the interconnects that pose the greatest timing problems. The wall layout now has the calorimetry front end electronics arranged in groups of racks. Between racks within these groups the trigger interconnects can still be easily made. We explore the possibility here of eliminating all other interconnects. Groups of racks are therefore isolated from each other, with no information passed as to the presence of any lateral EM showers. In the barrel region, these groups of racks would represent 4 calorimeter jet sums, covering a total area of (1.25, 1.25) in (η, ϕ). For the sake of this note, we term these groups of EM neighborhoods to be trigger 'towns'.

Figure 36 shows the effect on the background trigger rate for the baseline SP-veto single photon trigger. The rise in trigger rate is 40%. Figures 37 and 38 show the change in Higgs efficiency and top efficiency with the trigger towns. Figure 39 shows what one might expect, that at a particular background trigger rate, the actual effect on the Higgs efficiency is unchanged by breaking up the lateral veto neighborhoods into trigger towns.

Figure 40 shows the effect of the trigger towns on the background trigger

rate for the nominal EM-veto single photon trigger. The increase in rate is much less now, only 13% at the lower thresholds. This is not so surprising, since the number of EM cells effected is smaller. For the baseline SP-veto trigger, it is the 2 outside rings of EM sums in the town that are both effected by the lack of the lateral veto across the town boundary. In the EM-veto trigger, it is only the outside ring of EM sums that are effected. Also, the EM-veto trigger has a tighter area of lateral vetoing. A tighter lateral cut on one side would constrain neutral jets that presumably constitute many of the background triggers. By conservation of Pt around the jet core, a constraint on lateral energy on one side implies a constraint on the other side of the jet core.

Figure 41 shows the change in Higgs efficiency for the EM-veto trigger as a function of the the background trigger rate, with and without the trigger towns. The effect on the trigger performance is very small, even at the same trigger threshold. Given the currently foreseeable layout problems, we propose to incorporate these trigger 'towns' into the level one single photon trigger.

10 A Conglomerate Trigger

The performance of the single photon trigger combines the requirements of shower energy measurement, and isolation identification. Both considerations drive the segmentation to larger values, rather than smaller. At some segmentation size however, the accidental overlap with otherwise unrelated event background causes misidentification of both signal and background. In this section we consider a trigger that uses a larger segmentation for the shower energy measurement by applying the trigger threshold on the SPEM sums, and a smaller segmentation for the isolation identification by using the 8 neighboring EM sums for the lateral veto. This is a combination of the two previous lateral-veto trigger configurations discussed, and is still physically possible in the trigger hardware as is now foreseen.

The two conditions for this trigger still use the previous terminology of the isolated shower and the shared-shower, EMV1 and EMV2.

```
EMV1:
      (central SPEM greater than Pt threshold)
```

```
.and.  (1st largest EM neighbor is less than 1 GeV)

EMV2:
       (central EM sum is greater than 2/3 threshold)
.and.  (1st largest EM neighbor is over 1/3 threshold)
.and.  (2nd largest EM neighbor is less than 1 GeV)
```

In this scheme, the shower energy spread to neighboring EM sums is now counted in the total energy, where before it was lost. Of course, it must be below 1 GeV in any one sum, or be vetoed.

The Higgs performance of this trigger is shown in Figure 42, compared to the nominal EM sum lateral veto. The Higgs efficiency versus the background rate again follows the same curve as the previous cases, indicating little gain in trigger performance. The rates for a given energy threshold are somewhat higher.

As before, one could also provide for small shower spreading in the lateral veto constraint for the central isolated shower trigger. This is not quite like the previous case of the EM-sum trigger. There the isolated EM sum trigger was improved by leaving out one neighboring EM sum from the lateral veto, thereby gaining in those cases where shower spreading was self-vetoing an otherwise isolated photon. Here by leaving out one neighbor the effect is more ambiguous. This could be the neighbor to an isolated EM sum as before. But it could also be a shower-sharing neighbor within the SPEM sum, that hadn't otherwise met the 2/3 - 1/3 sharing criteria. While this might confuse the trigger cuts, it might lead to improved performance.

Figure 42 also shows this effect of leaving out the one EM neighbor for the isolated SP sum over threshold. There is an improvement in performance. As also shown in the figure a comparison with the nominal EM veto trigger with the one neighbor left unconstrained shows that the nominal trigger is still better, even if only that the background trigger rate is slightly lower for a given energy cut.

11 Conclusions

We have investigated the performace of the level-1 single photon trigger in detail, with respect to Higgs $\rightarrow 2\gamma$ efficiency. Several trigger schemes have

been simulated with QFL. The QFL shower parameterization was used for its much greater speed over other packages. Also the trigger segmentation is much coarser than a shower width, so one expects little dependence on the shower parameterization used. The two principle trigger schemes are the baseline (TDR) SPEM shower containment and lateral veto trigger, and a trigger using only the EM sums for the lateral veto and shower energy containment.

Several sources are responsible for the loss in Higgs efficiency. One class is that due to event related overlap. This can veto an otherwise isolated photon, by the chance overlap of a jet. Our studies have shown that this is at a low level for the nominal .157 x .157 segmentation.

The other class of inefficiencies is that due to shower self-vetoing. Photons near to the trigger threshold suffer an unavoidable loss due to the sharing of EM showers between trigger sums. The nominal trigger allows for sharing between 2 trigger sums, but even for showers that share between 2 sums there is a class of sharing that is missed by the discriminator trigger scheme. Near threshold, the efficiency of this trigger scheme is about 60%.

For photons further from the trigger threshold ($\geq$ 10 GeV over threshold) another inefficiency becomes dominant, shower spreading. This inefficiency makes an isolated photon appear to be spread over more than 2 trigger sums, and the lateral isolation requirement forces a veto. This would be true of any 2-sum trigger scheme. By using simple logic in the discriminator based trigger we can mitigate this effect, by leaving out the veto constraint on one EM trigger neighbor, when the central EM sum is fully over threshold. This modification though gives the best trigger performance, with an improved Higgs efficiency at a given background trigger rate.

The size and threshold used for the hadronic veto behind the EM energy deposit has little effect on trigger efficiency or background rate. For the nominal segmentation, there is very little dependence of the trigger efficiency or background rate on rapidity. A study of the offsets of the channel-to-channel dispersion of the preamplifier gains indicates that the trigger performance is insensitive to this, and the discriminator turn-on curve is essentially unmodified for a dispersion of gains of 5% or less.

We have also explored other trigger segmentations, smaller and larger than the nominal. At very large segmentations, the trigger becomes sensitive to unrelated event overlap. At small segmentations, the containment suffers as the shower spreads easily over 2 or more EM sums. The .157 x .157

segmentation is near to optimal, and the easiest to implement in hardware.

One problem that has been explored is that of the trigger timing. The interconnects between trigger racks that carry the information for the lateral shower isolation require more time than can be allowed for in the 2 μsec trigger latency. By grouping the lateral shower isolation into groups of 4 jet sums, or (1.25, 1.25) in (eta, phi), one finds little change in trigger performance for the nominal EM lateral veto scheme. We propose to implement these "trigger towns" in the level 1 photon trigger.

Figure 43 and the corresponding Table 2 show a summary of the different trigger configurations modelled, and the actual performance of the trigger in Higgs efficiency versus the background trigger rate. The parameter being varied is actually Pt threshold, for each of the functions of efficiency and background rate. One sees an interesting curve that is insensitive to the exact cuts used by the trigger for the EM lateral veto trigger. The Pt threshold determines the point along the curve that the trigger actually falls, but the shape is reasonably "universal".

We have used this curve as the principle criterion in gauging trigger performance. This shows that most parameters that one might vary to optimize the trigger performance are moot. Gains or losses in efficiency are followed by a corresponding loss in rate. It is also desirable to have a particular efficiency and rate at the lowest energy threshold possible, of course. Almost every trigger configuration explored in this curve however has the highest efficiencies at reasonably low energy thresholds, which makes energy threshold a weak criterion for trigger selection.

There are a few trigger configurations that are notable exceptions to the "universal" curve. The one falling lower, curve "b", is that of the TDR-baseline SPEM trigger. We propose to drop the SPEM trigger, in favor of the EM sum trigger scheme. The highest curve on this plot, curve "e", corresponds to the nominal EM trigger with one neighbor left out of the isolated EM sum lateral veto. The one curve that falls in between, curve "c", corresponds to a somewhat larger trigger segmentation, the .209 x .209. This leads to better shower containment, and obviates some of the self-vetoing due to shower spreading. The loosened isolation veto in curve "e" is designed to address just this inefficiency, and performs better over a larger range of energy thresholds. We propose to implement this loosened isolation veto in the level 1 trigger.

The trigger scheme proposed here, that of the EM sum lateral veto,

with one neighbor unconstrained when the central sum is fully over threshold, and with one hadronic SP sum for the longitudintal vetoing, provides near-optimal trigger performance. It is possible that some other scheme can achieve similar Higgs $\rightarrow 2\gamma$ efficiency for a similar background trigger rate, at a lower Pt threshold. However, many of the dependences of the trigger performance are weak, even that of Pt threshold for broadly similar trigger conditions. Further improvements could only come from a trigger using much more shower information, such as recognizing 3- and 4-EM sum showers, though even these improvements would be modest at best. By lowering the trigger threshold $\approx$ 10 GeV below the desired threshold and accepting the background rate, one already has a first level trigger that is almost fully efficient for single photons.

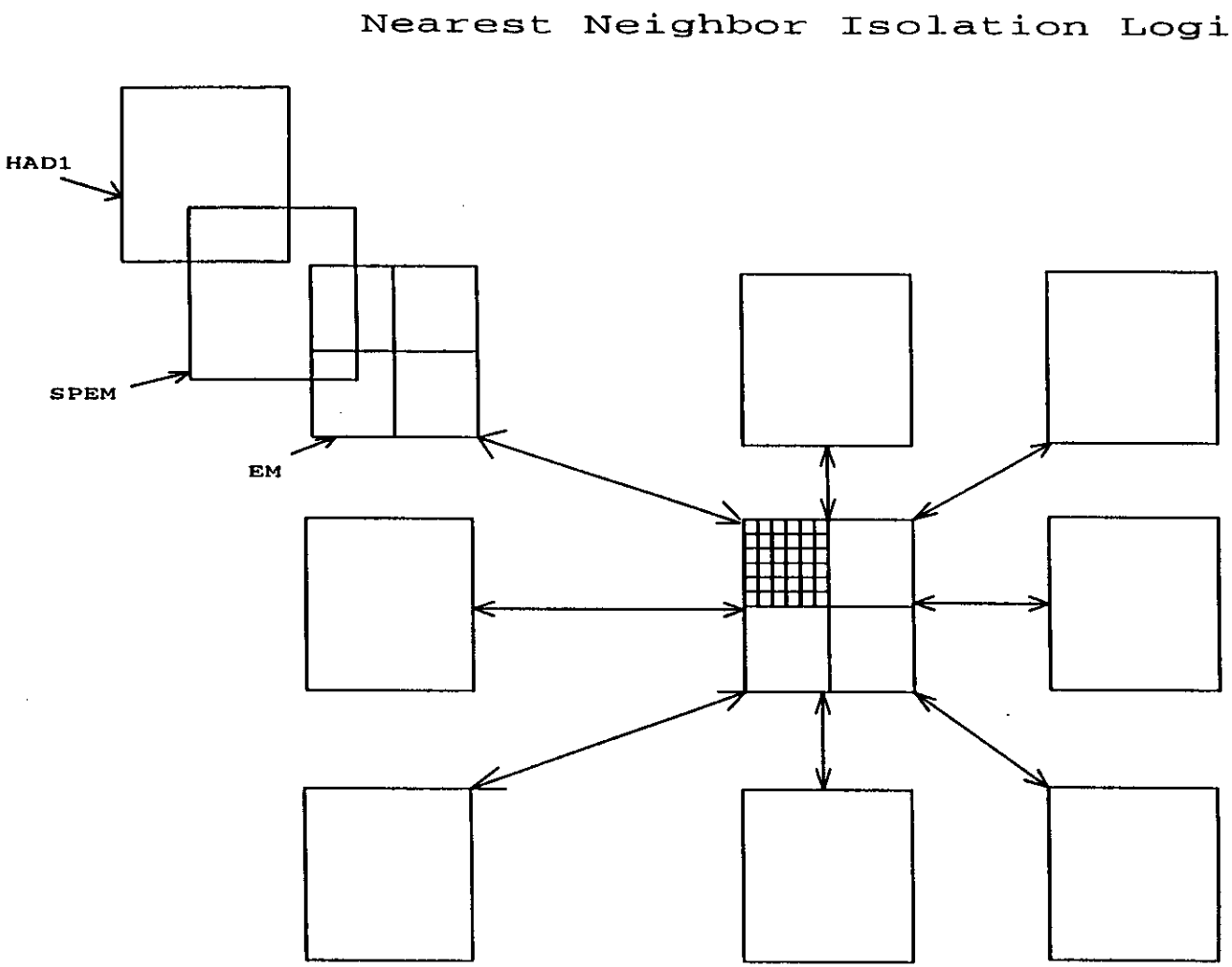

Figure 1: The Baseline Trigger Algorithm. This shows the relationship between the EM sums and the SP sums in the photon trigger.

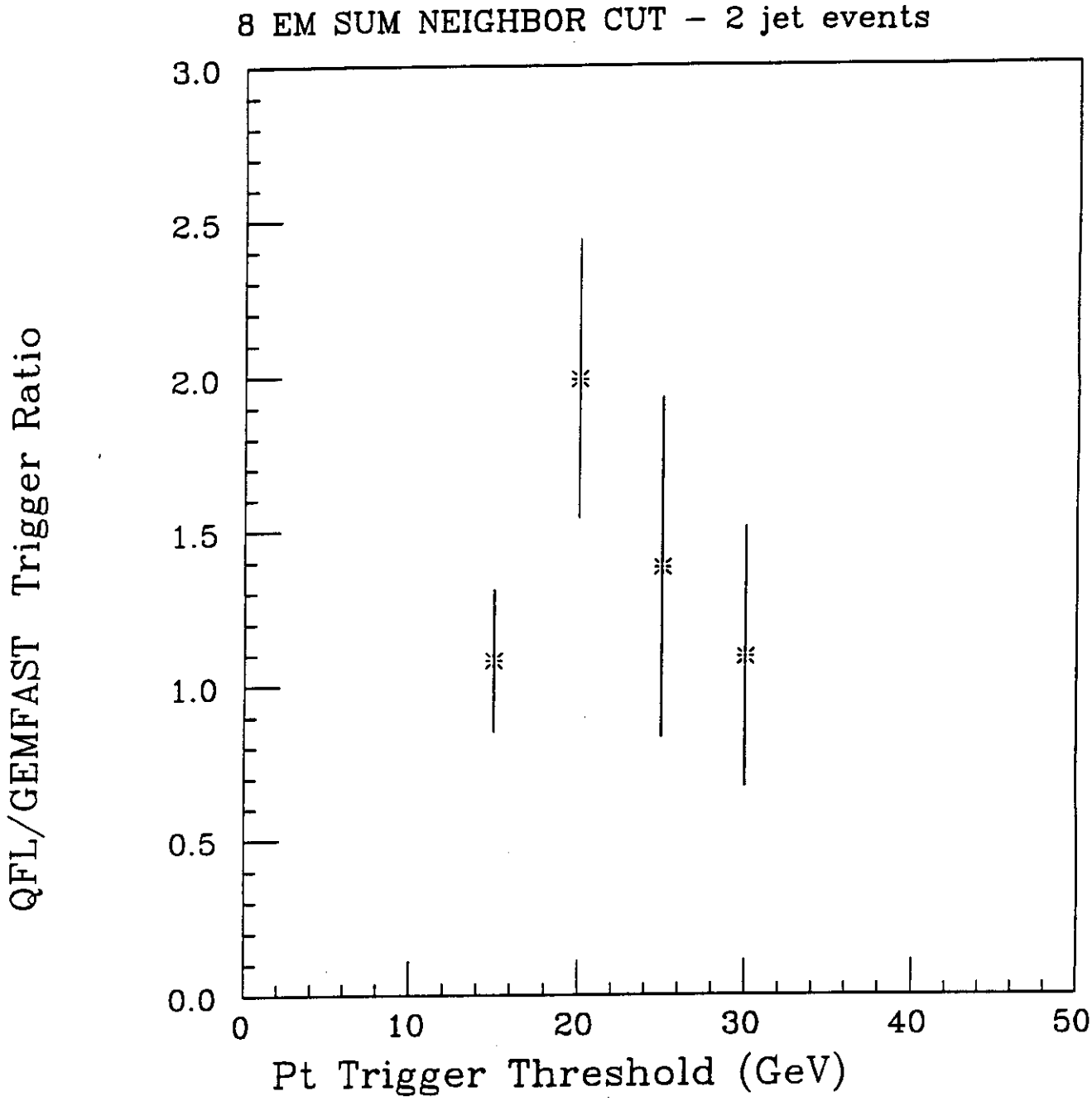

Figure 2: Comparison of QFL and GEMFAST. Background trigger rates are compared for the two simulations at several trigger thresholds.

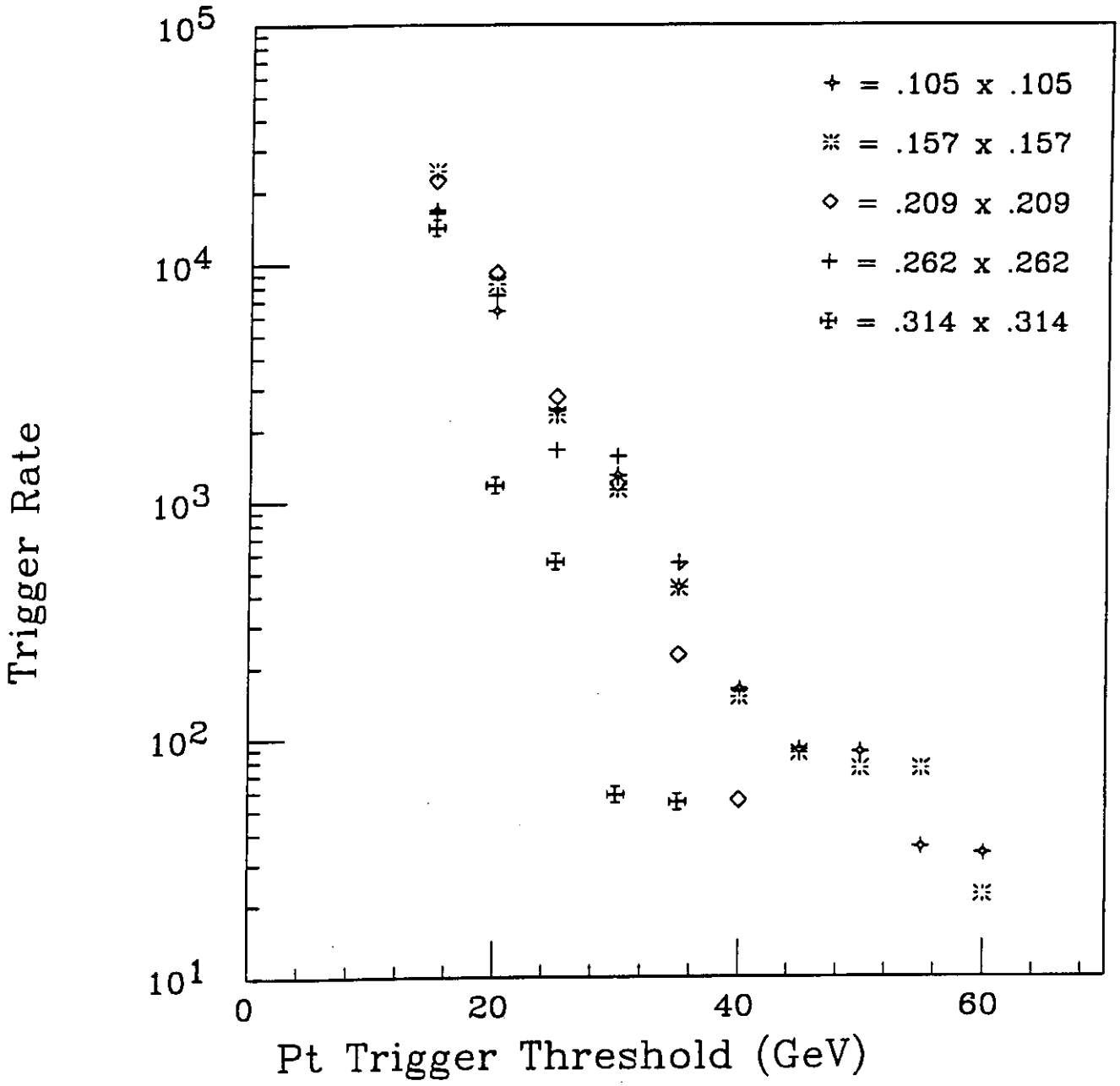

Figure 3: Background Trigger rate for baseline single photon trigger. The nominal segmentation of .157 competes with the .209 segmentation for the highest trigger rate.

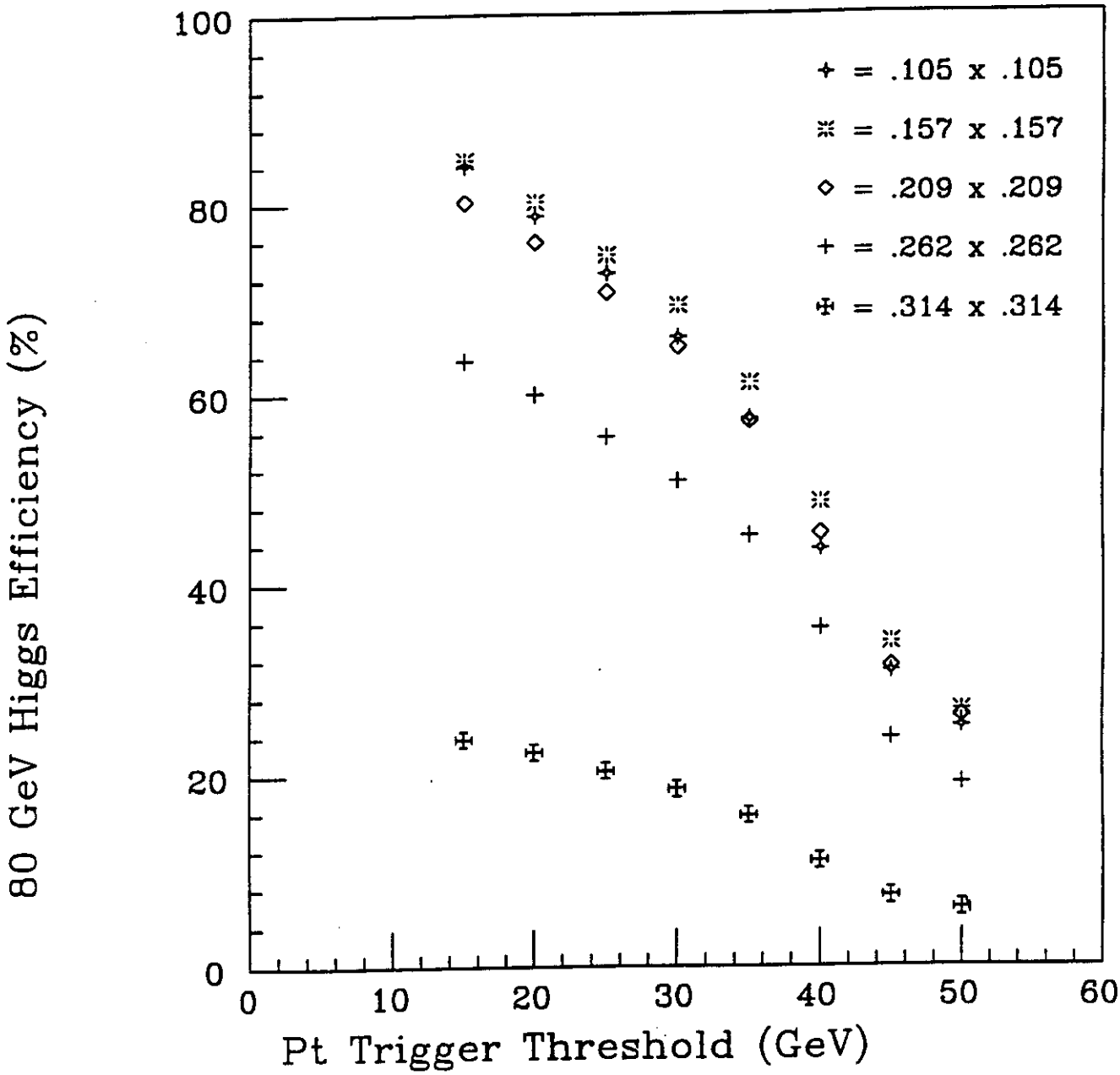

Figure 4: Efficiency for an 80 GeV Higgs with the baseline single photon trigger. Each trigger threshold bin is normalized to the number of events with at least 1 Higgs decay photon above that energy. The nominal segmentation of .157 gives the highest efficiency at the lower trigger thresholds.

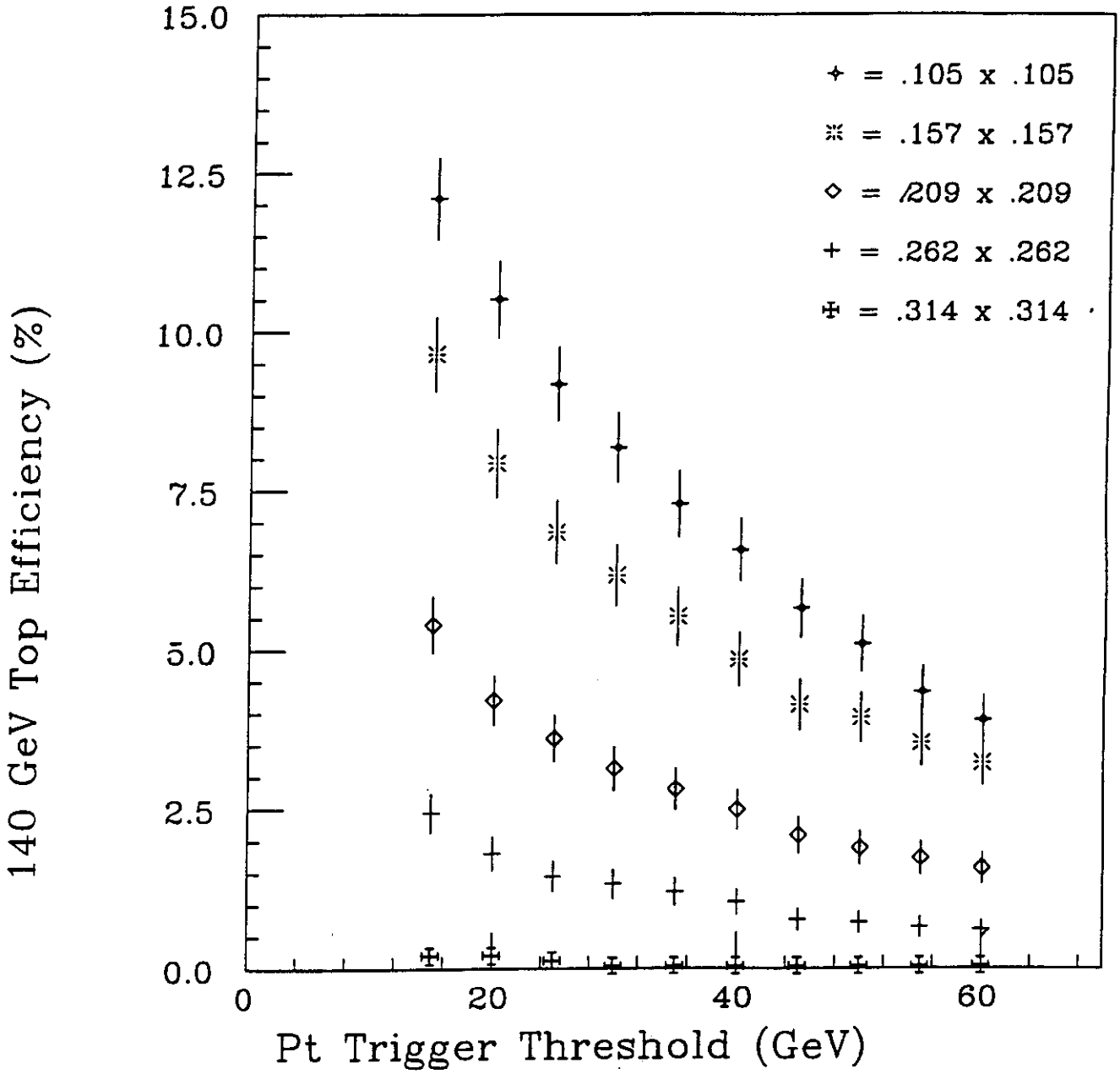

Figure 5: Efficiency for a 140 GeV Top quark with the baseline single photon trigger. The branching ratios for the semi-leptonic decays are included. The top quarks are produced with a minimum of 100 GeV Pt. The smallest segmentation shows the best efficiency, since there are nearby energy deposits associated with the jet.

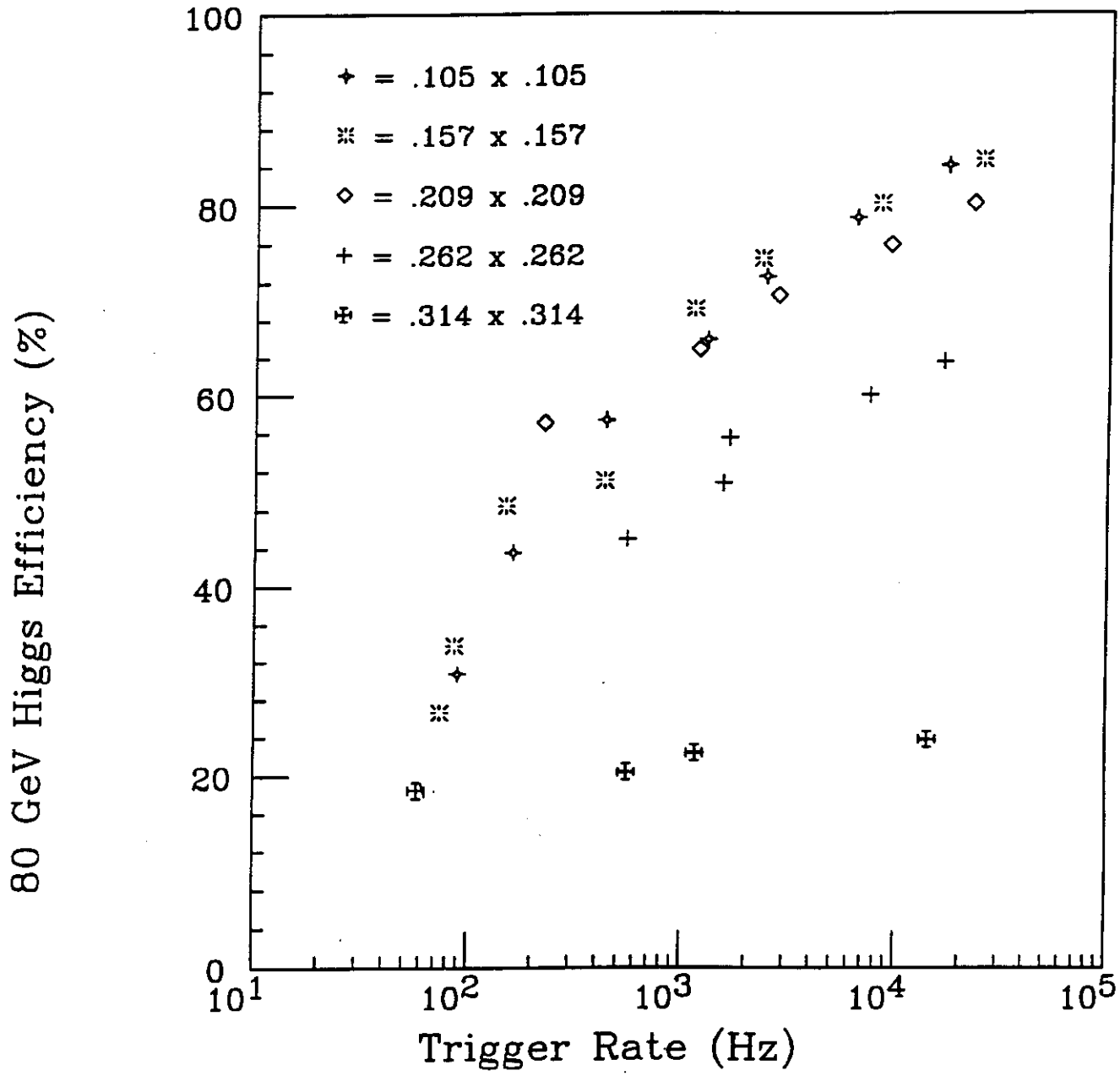

Figure 6: The Higgs Efficiency versus background trigger rate for the baseline single photon trigger. At a given 1st level trigger rate, it is best to maximize the efficiency for Higgs. The 2 smaller segmentations give the best efficiency.

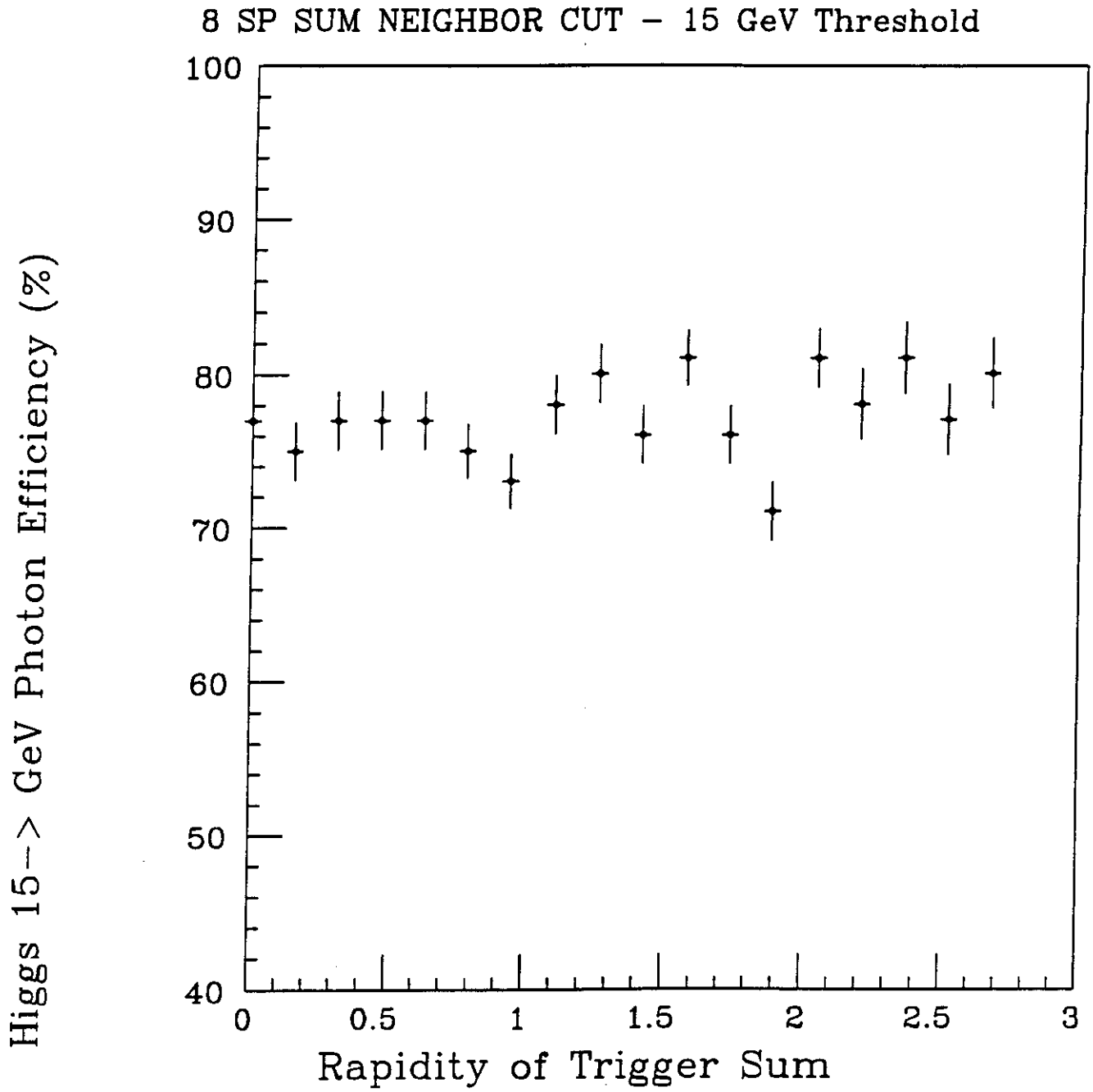

Figure 7: The baseline single photon trigger efficiency as a function of rapidity. The photons above 15 GeV from the Higgs data set were used, with a trigger threshold of 15 GeV. Within statistics, the trigger efficiency is flat with rapidity. The average of these data points is only 77 %.

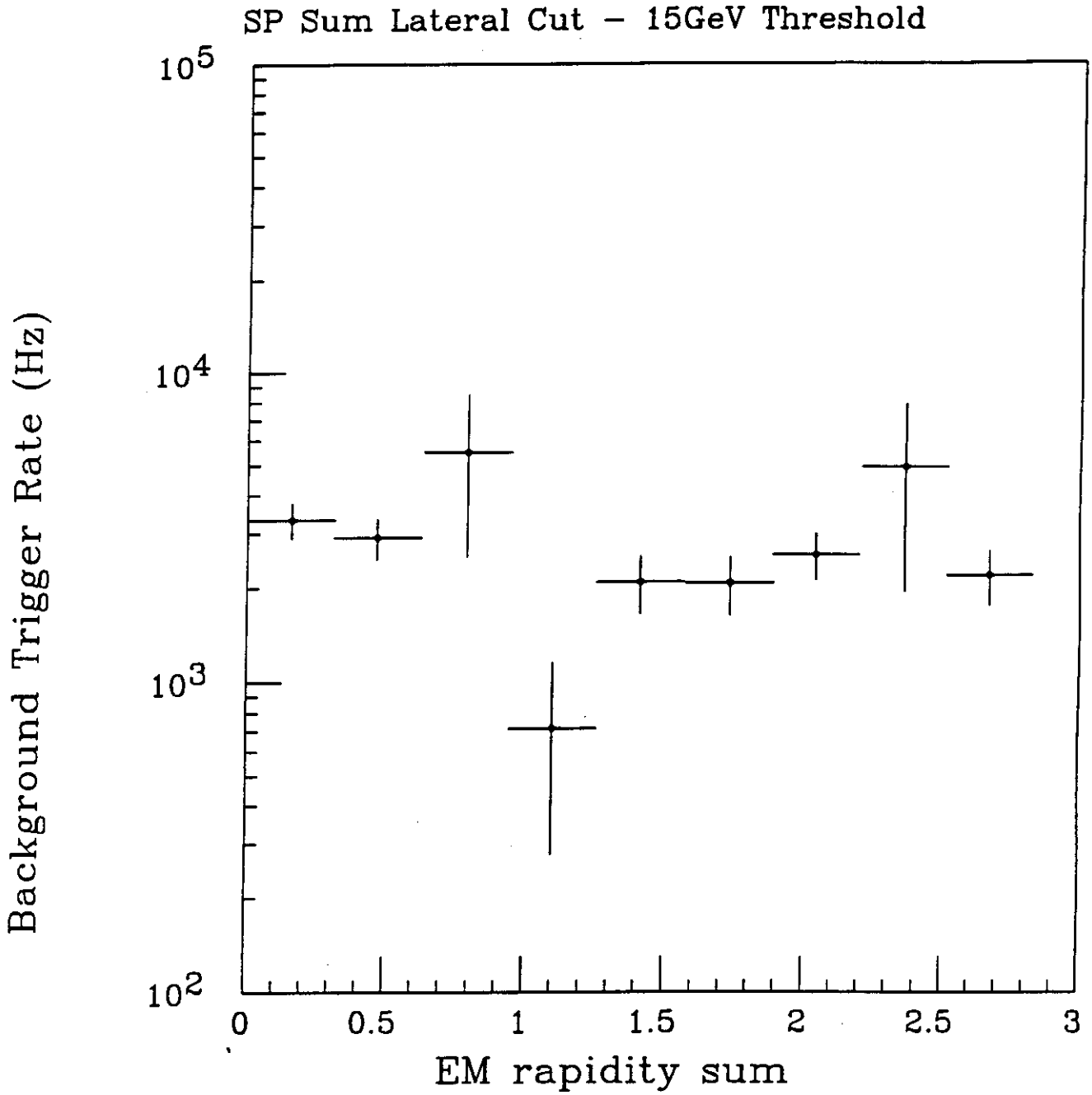

Figure 8: The background trigger rate as a function of rapidity for the baseline single photon trigger at a threshold of 15 GeV. The background triggers seem flat with rapidity, within statistics. There is no gap here between the barrel and the endcap, contrary to what may seem indicated.

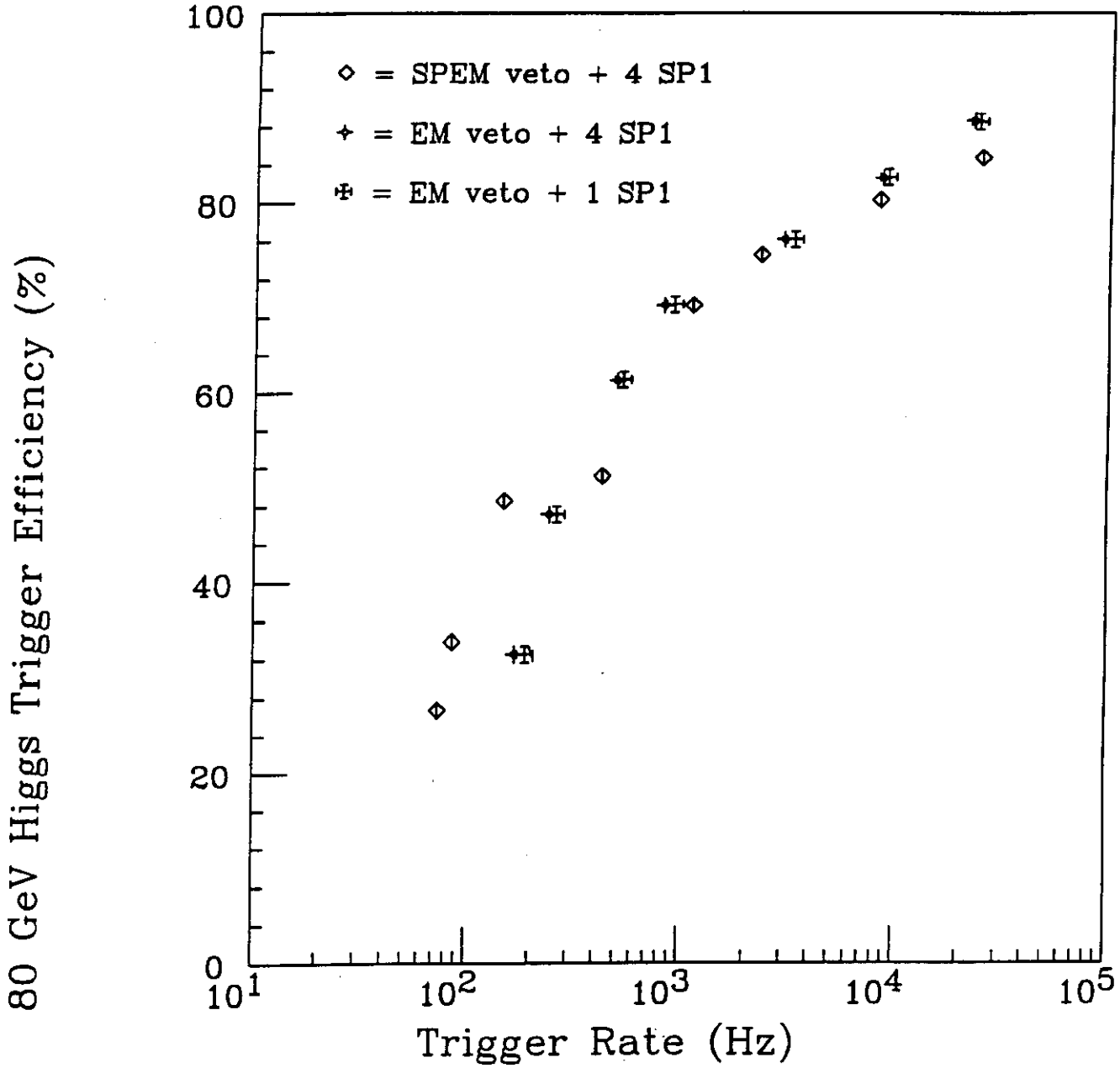

Figure 9: The Higgs Efficiency versus the background trigger rate for two single photon trigger schemes, compared to the baseline. The SPEM scheme is the baseline, while the EM uses the 8 neighboring EM trigger sums for the lateral veto. For a given 1st level trigger rate, the efficiency for Higgs is very similar, with perhaps some improvement at the lowest energy thresholds (highest trigger rates). There is little difference between using the 4 hadronic SP sums and using the 1 hadronic SP sum immediately behind the trigger EM sum for the hadronic veto.

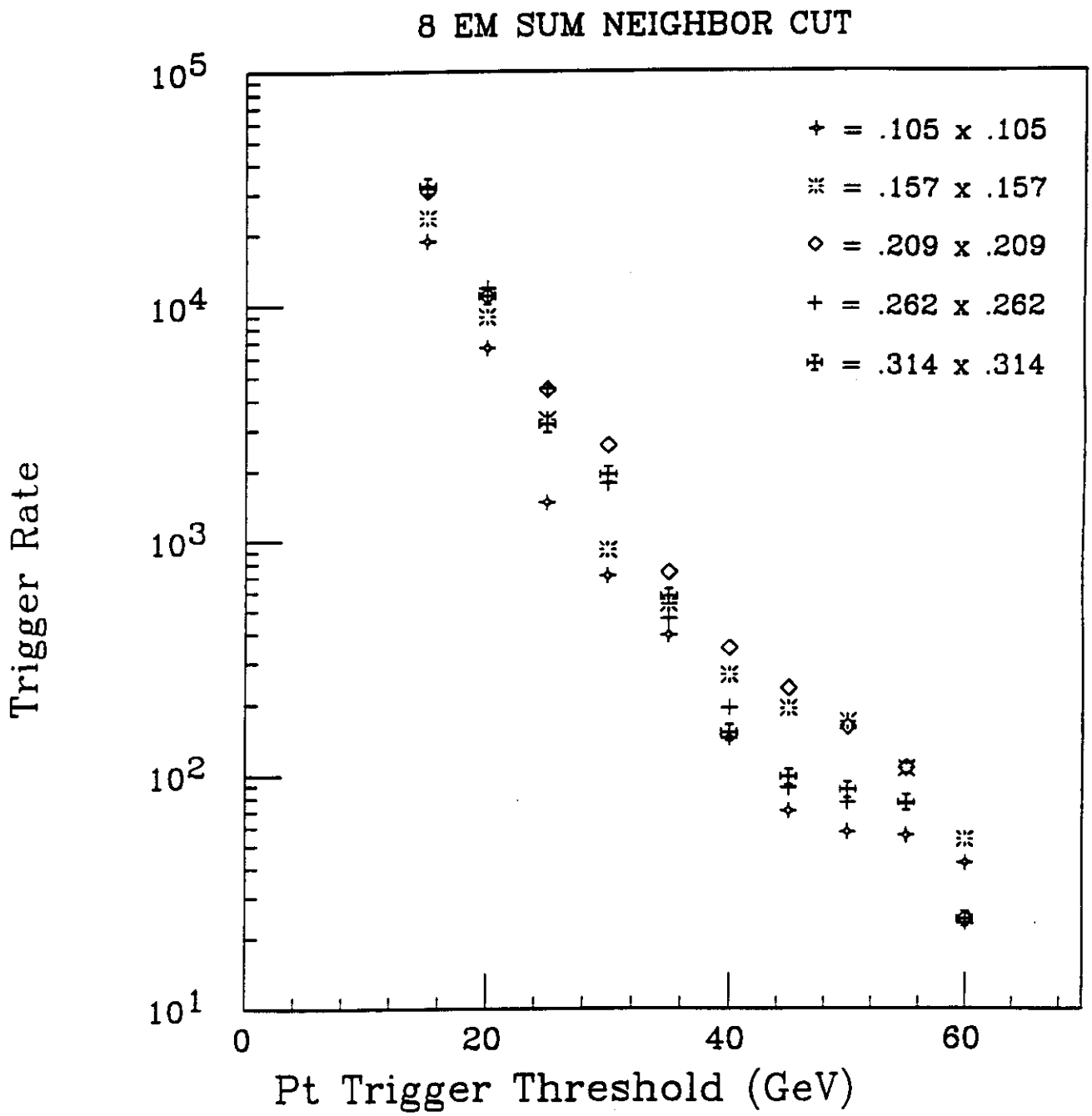

Figure 10: The background trigger rate for the EM-veto single photon trigger. The trigger rate for the nominal segmentation has changed very little at the lowest thresholds, but no longer gives the highest trigger rates. The larger segmentations now have the ability to contain more energy without being penalized as quickly for having much larger lateral veto regions.

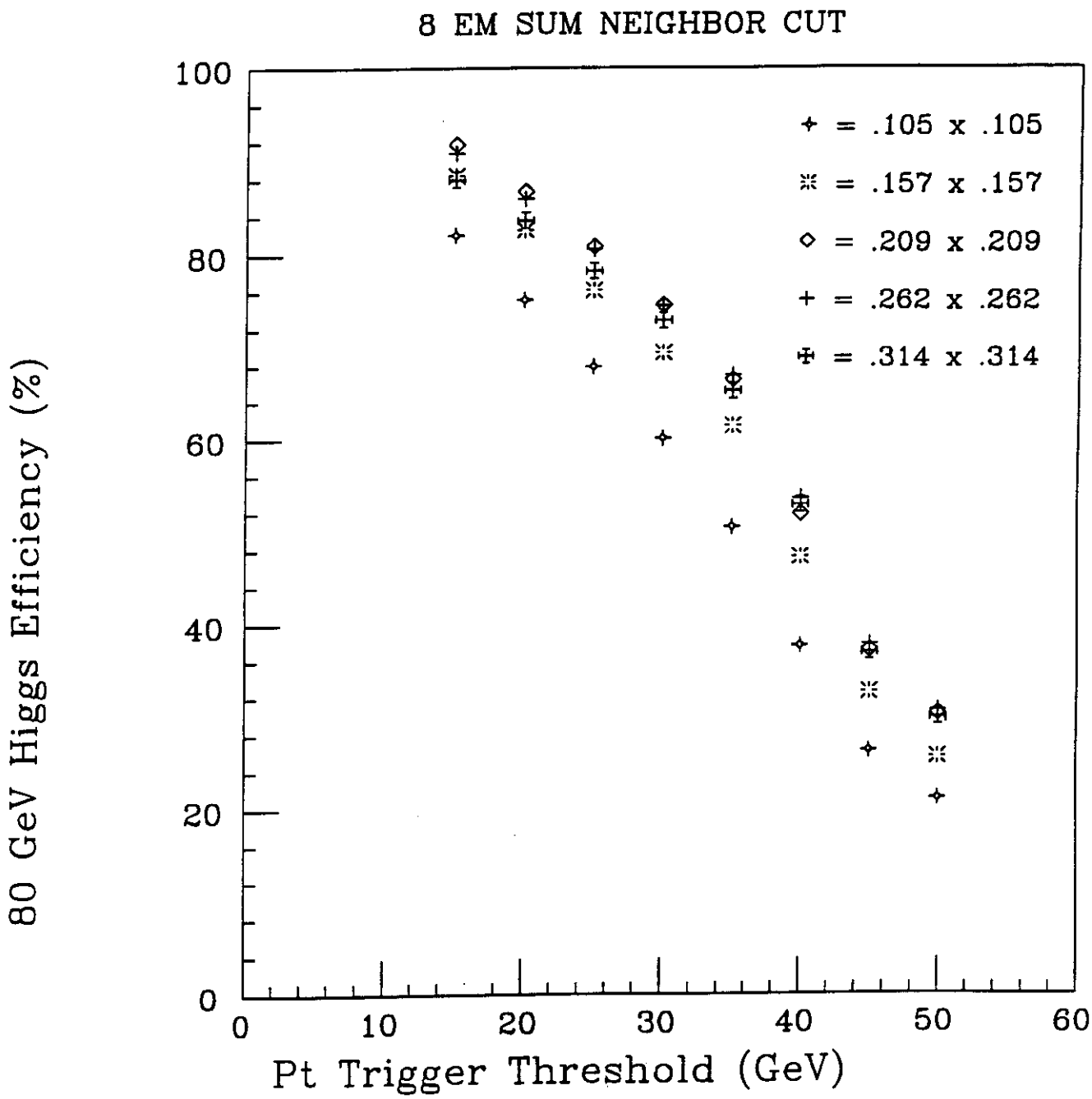

Figure 11: The Efficiency for a 80 GeV Higgs with the EM-veto single photon trigger. The nominal segmentation now shows a better efficiency at a given energy threshold than with the baseline trigger, but no longer gives the best efficiency at that threshold.

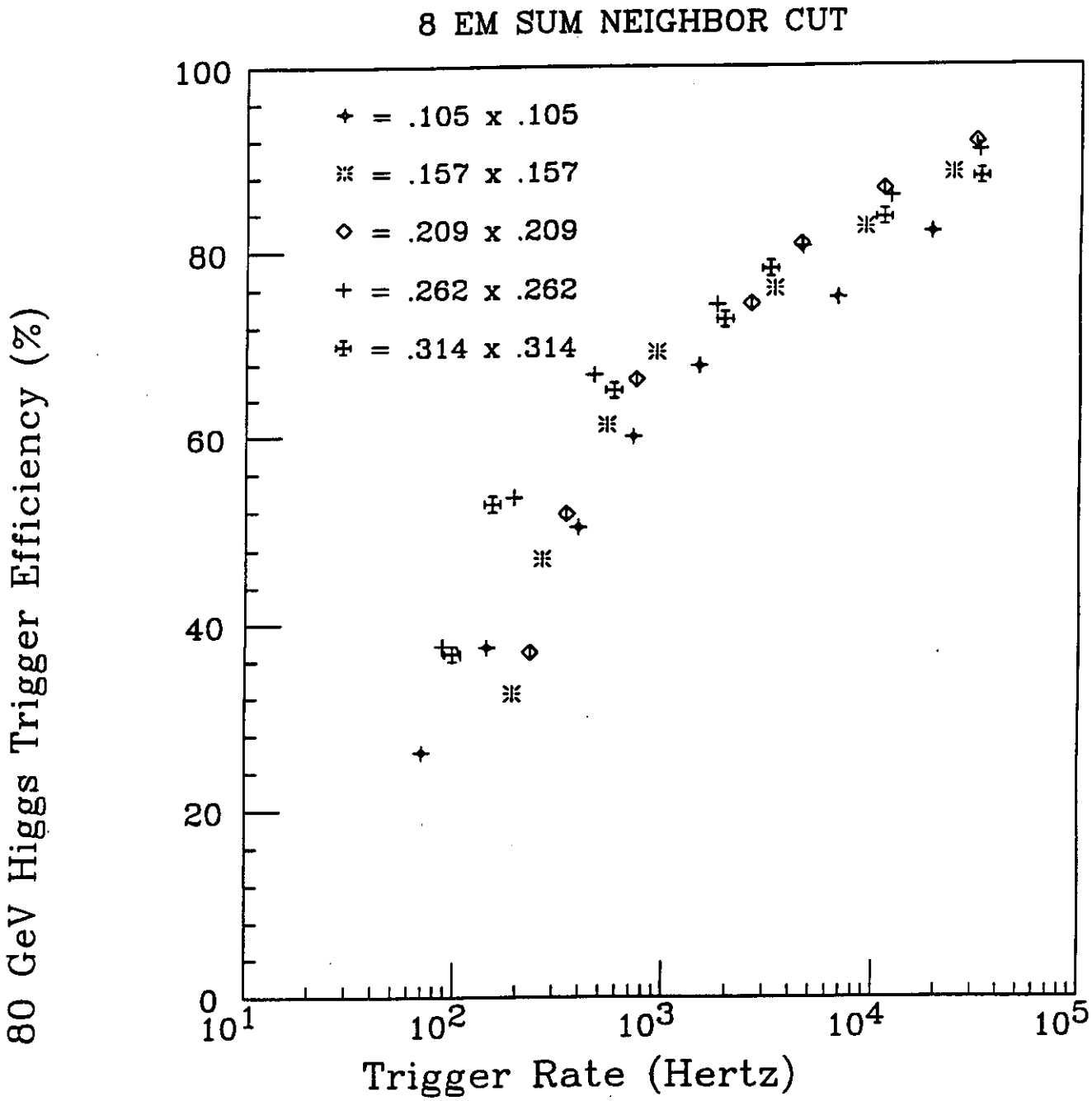

Figure 12: The Higgs Efficiency for the EM-veto single photon trigger versus the background trigger rate. Aside from the smallest segmentation, the results bunch up along a single curve, and are insensitive to the segmentation size. The .209 size gives the slightly better performance.

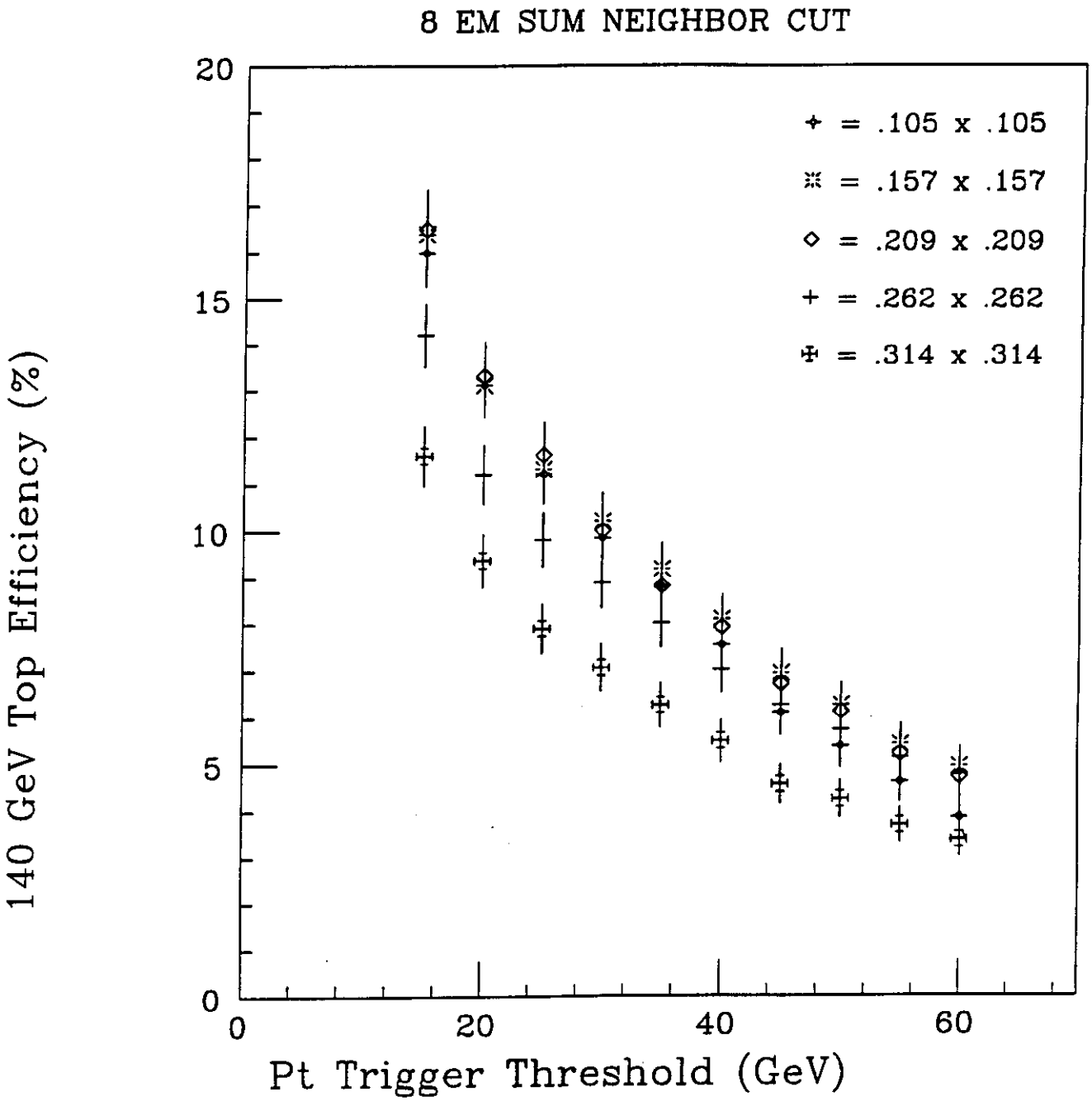

Figure 13: Efficiency for a 140 GeV Top quark with the EM-veto single photon trigger. The branching ratios for the semi-leptonic decays are included. The top quarks are produced with a minimum of 100 GeV Pt. All 3 of the smaller segmentations now show the best efficiency.

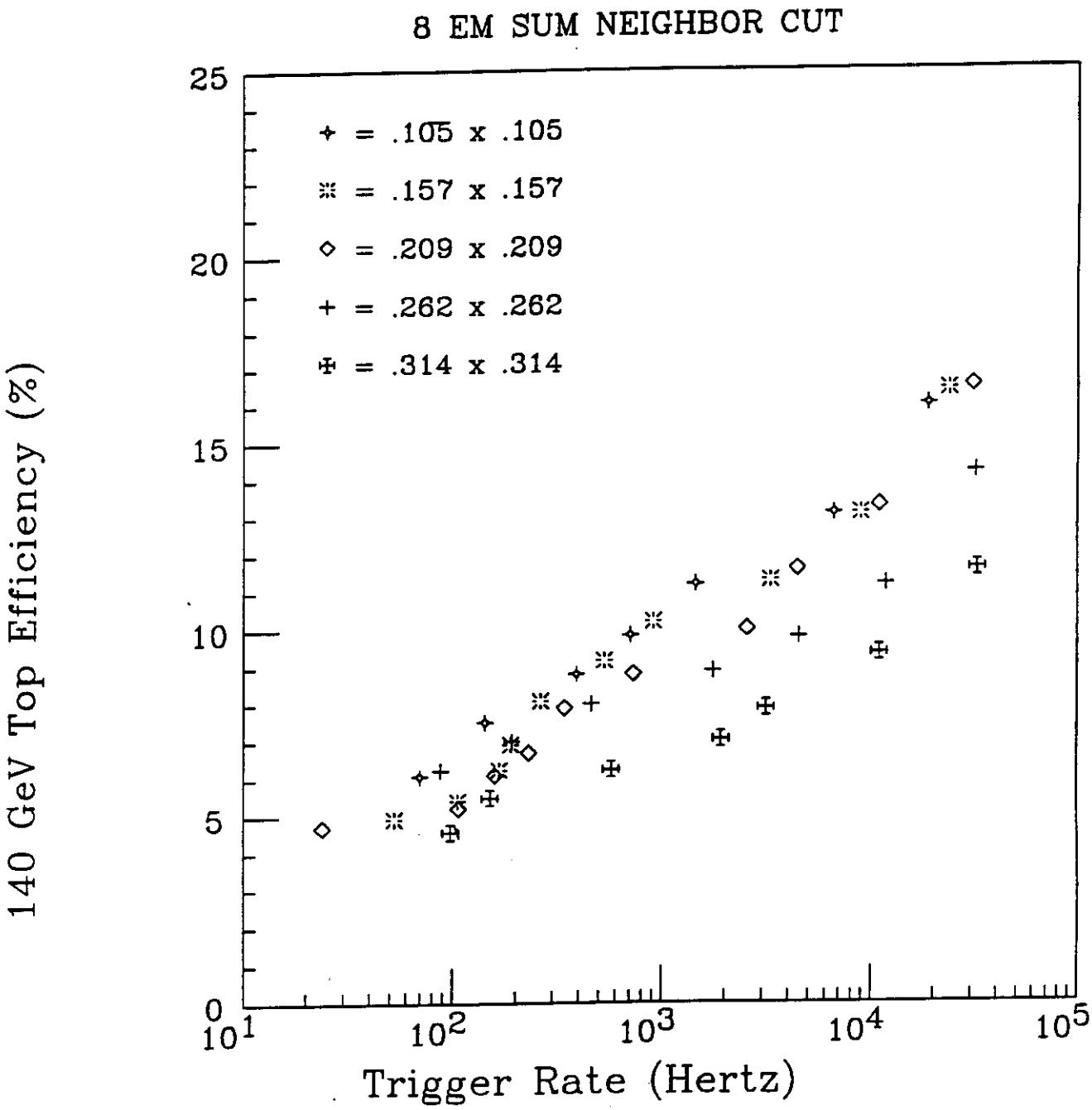

Figure 14: The Top Efficiency for the EM-veto single photon trigger versus the background trigger rate. The smaller segmentations give the better performance.

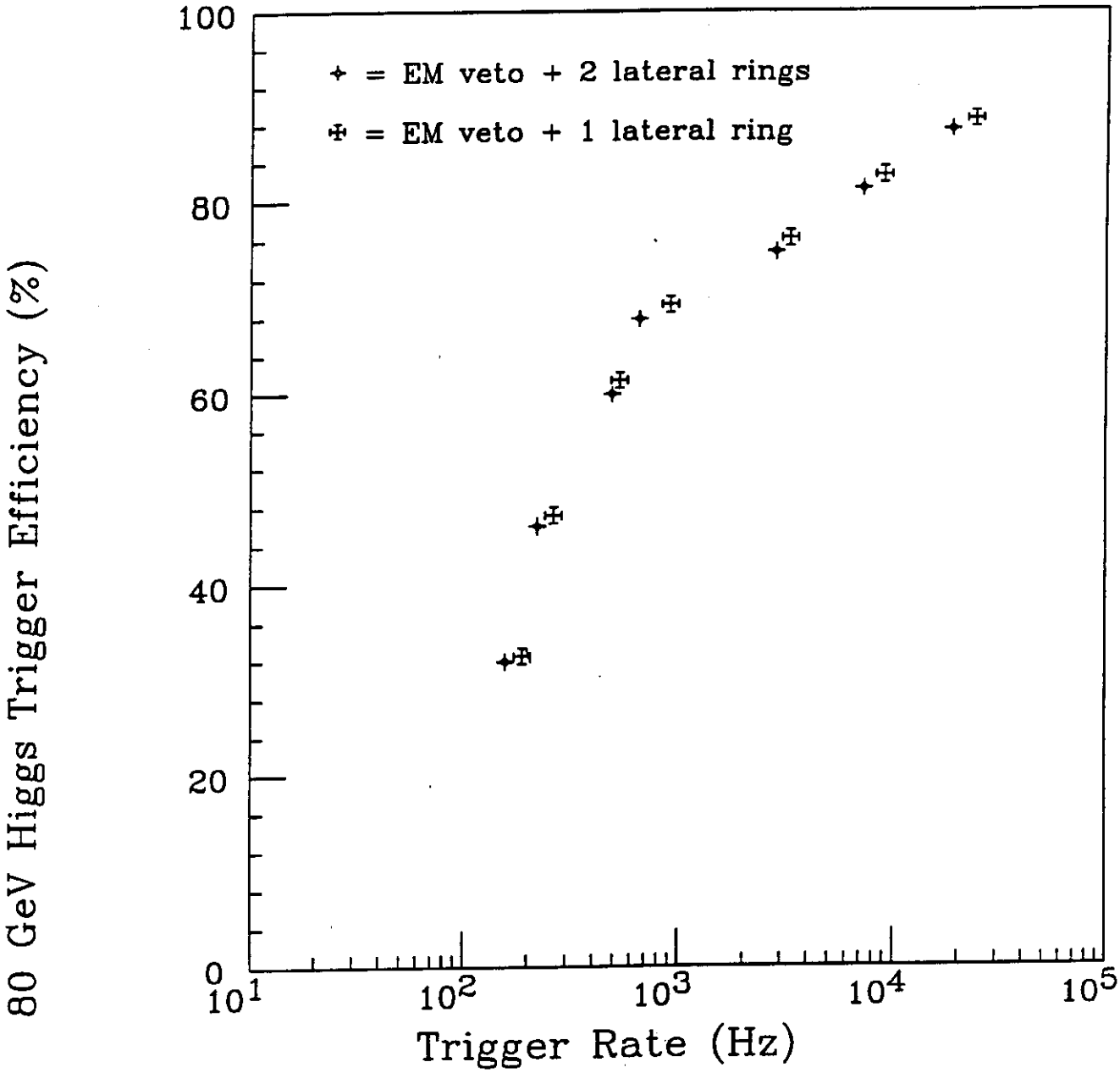

Figure 15: The Higgs Efficiency versus the background trigger rate for the single photon trigger. Here the EM-veto scheme using 1 ring of 8 neighboring EM sums for the lateral veto is compared against a similar photon trigger using 2 rings of EM sums for the lateral veto. The second ring is always required to have all EM sums below 1 GeV. While there is some improvement in background rate at a given energy threshold, there is also a corresponding drop in Higgs efficiency. The two cases fall on the same curve above, showing no overall benefit from using 2 rings.

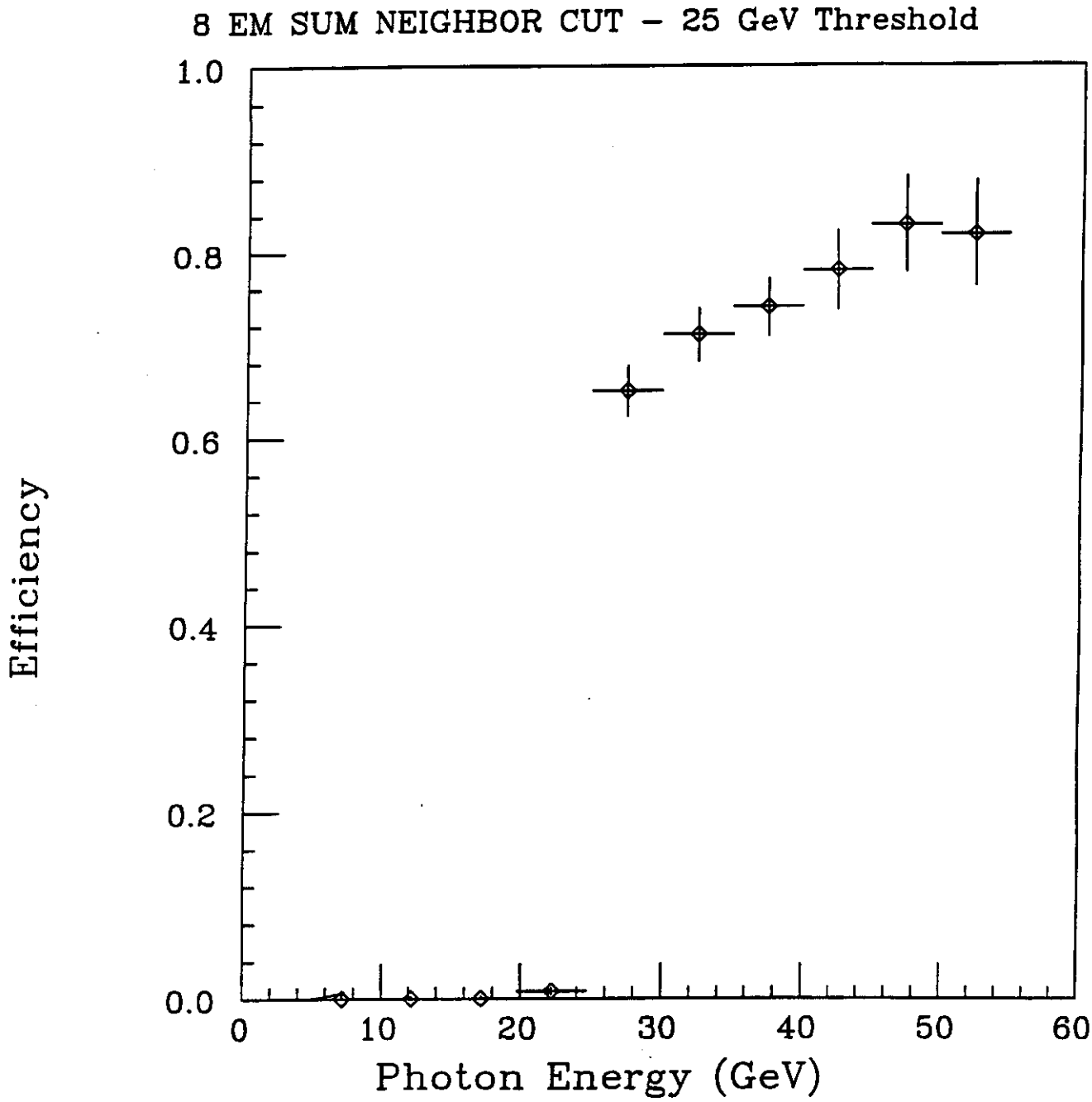

Figure 16: The trigger response as a function of photon energy, showing the photon efficiency for a trigger threshold of 25 GeV. There is a sharp rise in the photon efficiency at threshold, with a shoulder up to the full efficiency.

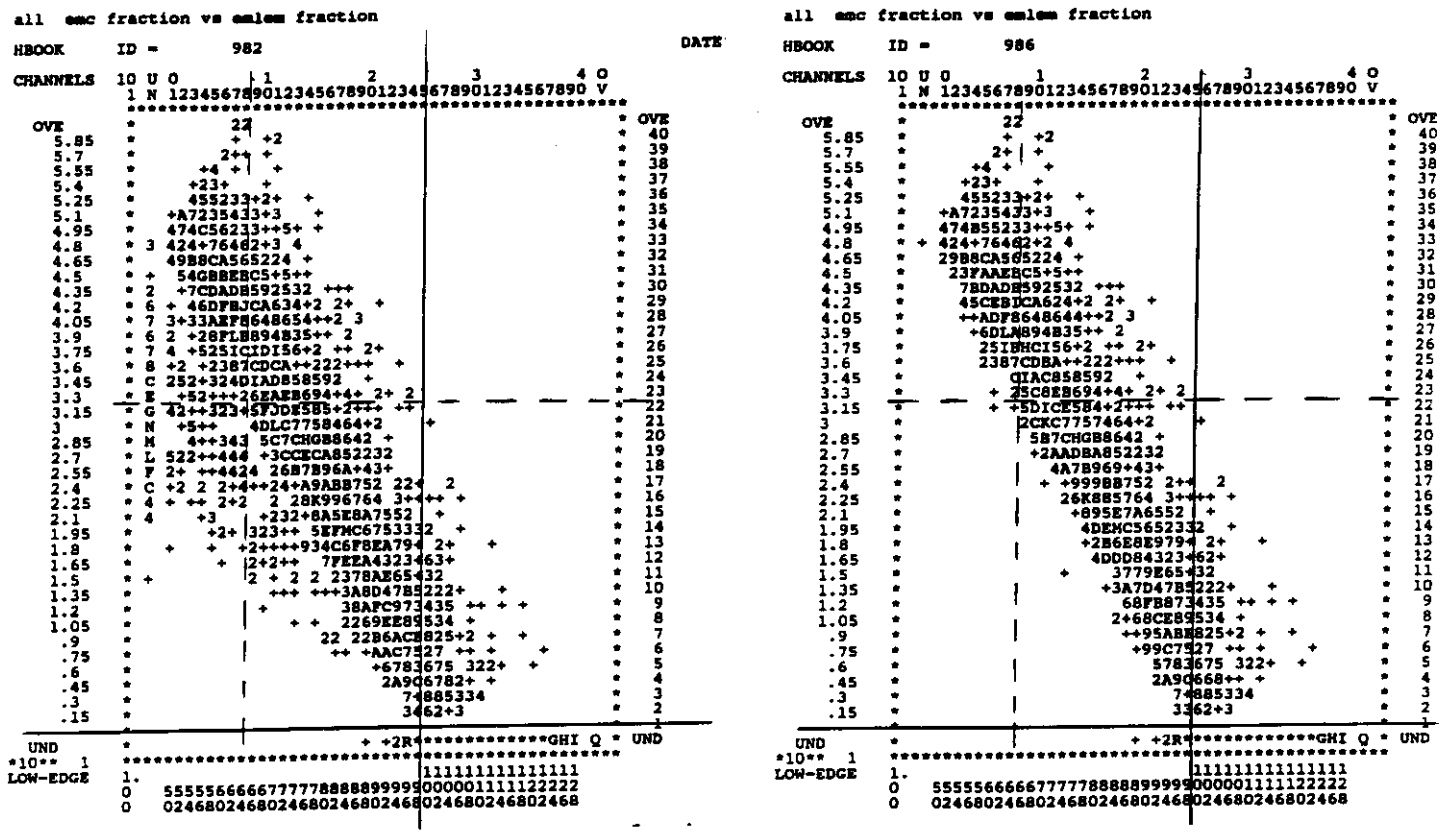

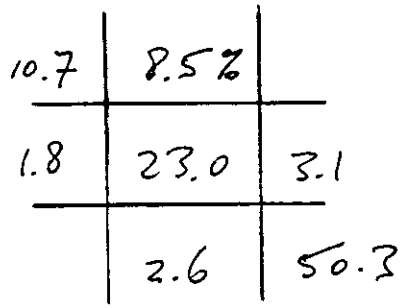

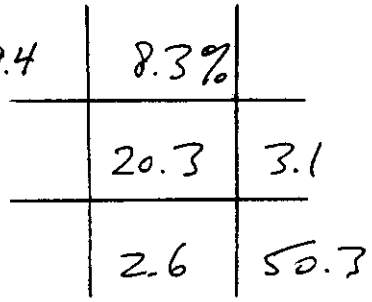

Figure 17: The photon shower sharing between the central EM sum and the highest neighbor in energy. The bottom axis is the central EM sum energy normalized to trigger threshold, and the vertical axis is that of the highest neighboring EM sum also normalized to trigger threshold. The EM showers in this plot are all over threshold, but less than 5 GeV over. The plot on the right requires the other 7 neighbors to be less than 1 GeV. The solid lines demonstrate the action of the isolated EM-shower trigger, the dashed line the EM-sum sharing trigger. The single photon trigger is represented by the two sets of showers combined.

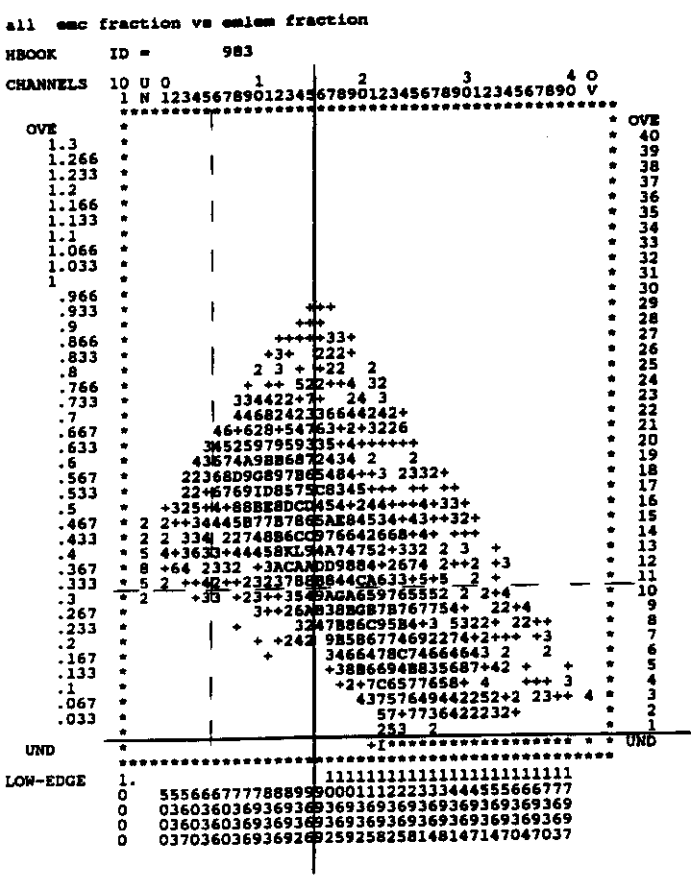

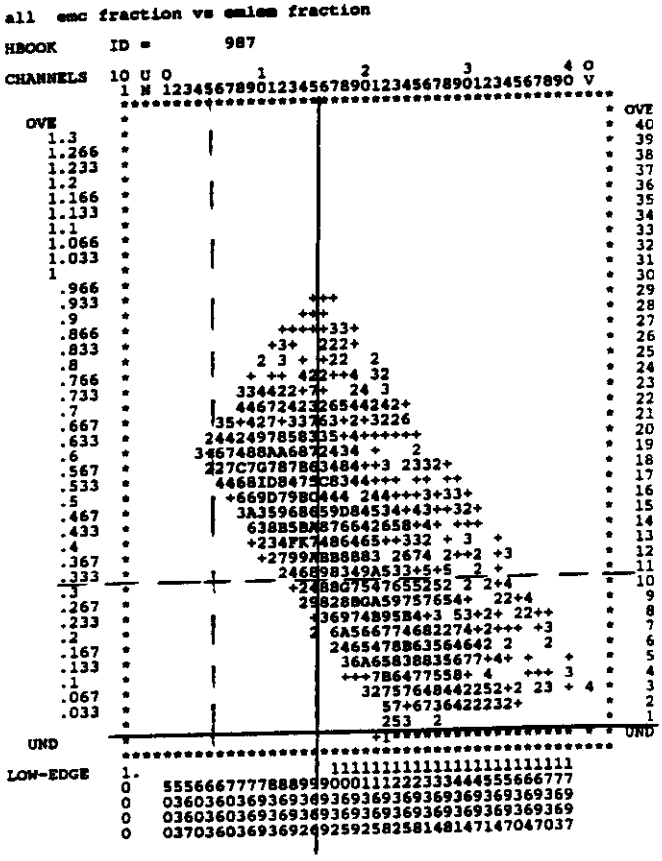

1.9	16.4	11.8%
0.1	1.2	16.3
		52.2

0.2	13.6	11.1%
	0.4	15.1
		52.2

Figure 18: The photon shower sharing between the central EM sum and the highest neighbor in energy. The bottom axis is the central EM sum energy normalized to trigger threshold, and the vertical axis is that of the highest neighboring EM sum also normalized to trigger threshold. This is the same as Figure 17, only here the EM showers are restricted to the range 10-15 GeV over threshold. The plot on the right requires the other 7 neighbors to be less than 1 GeV. The solid lines demonstrate the action of the isolated EM-shower trigger, the dashed line the EM-sum sharing trigger. The single photon trigger is represented by the two sets of showers combined.

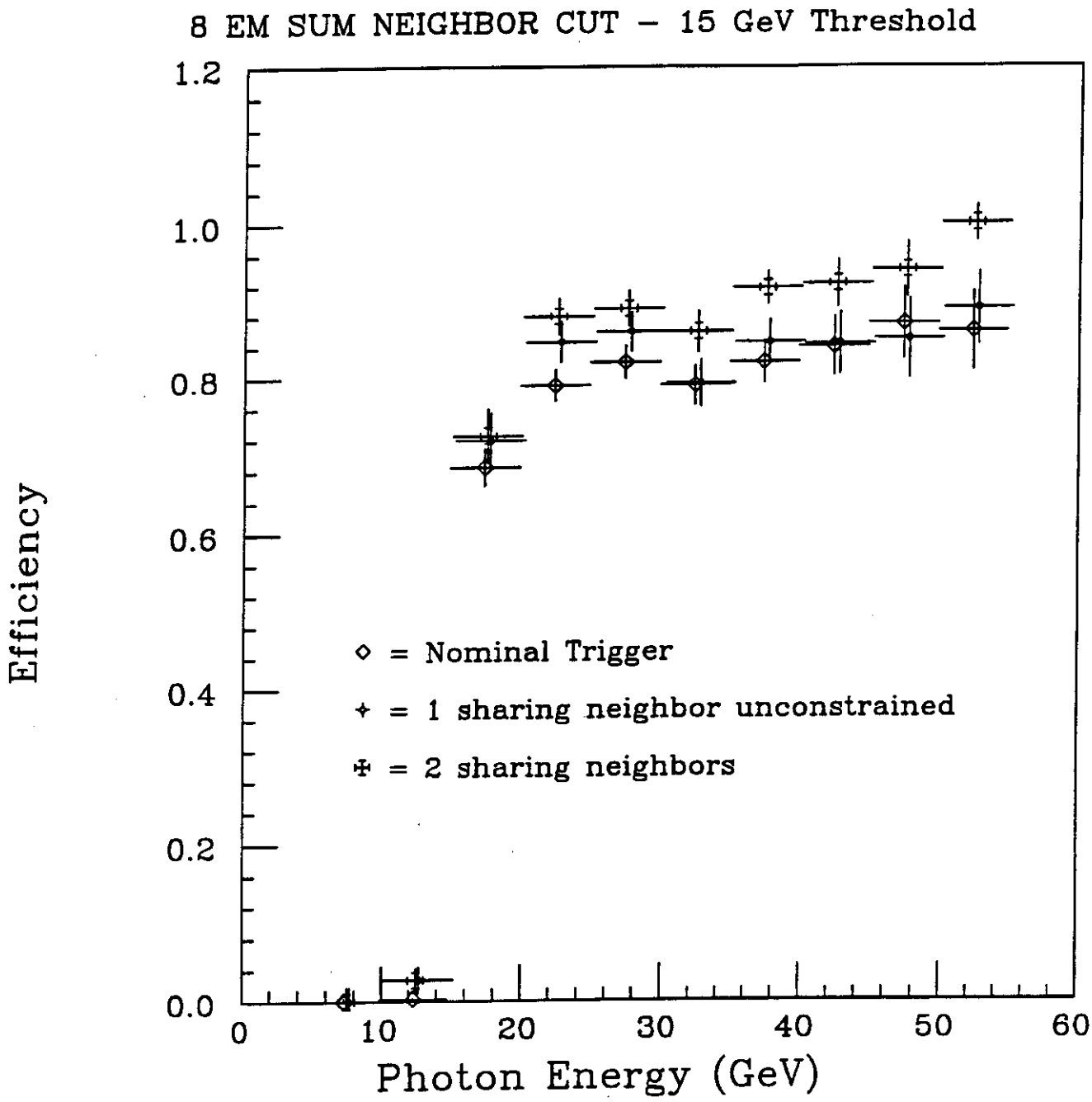

Figure 19: The trigger response as a function of photon energy, showing the photon efficiency for a trigger threshold of 15 GeV. The nominal EM-veto trigger is shown along with the curves for leaving 1 and 2 EM sums out of lateral veto. These are left out for the 2 EM sum sharing part of the trigger only. The EM sums left out of the lateral veto were chosen by those that had the most energy of all of the neighbors. The plateau efficiency is improved somewhat for the case of 2 EM sums left unconstrained.

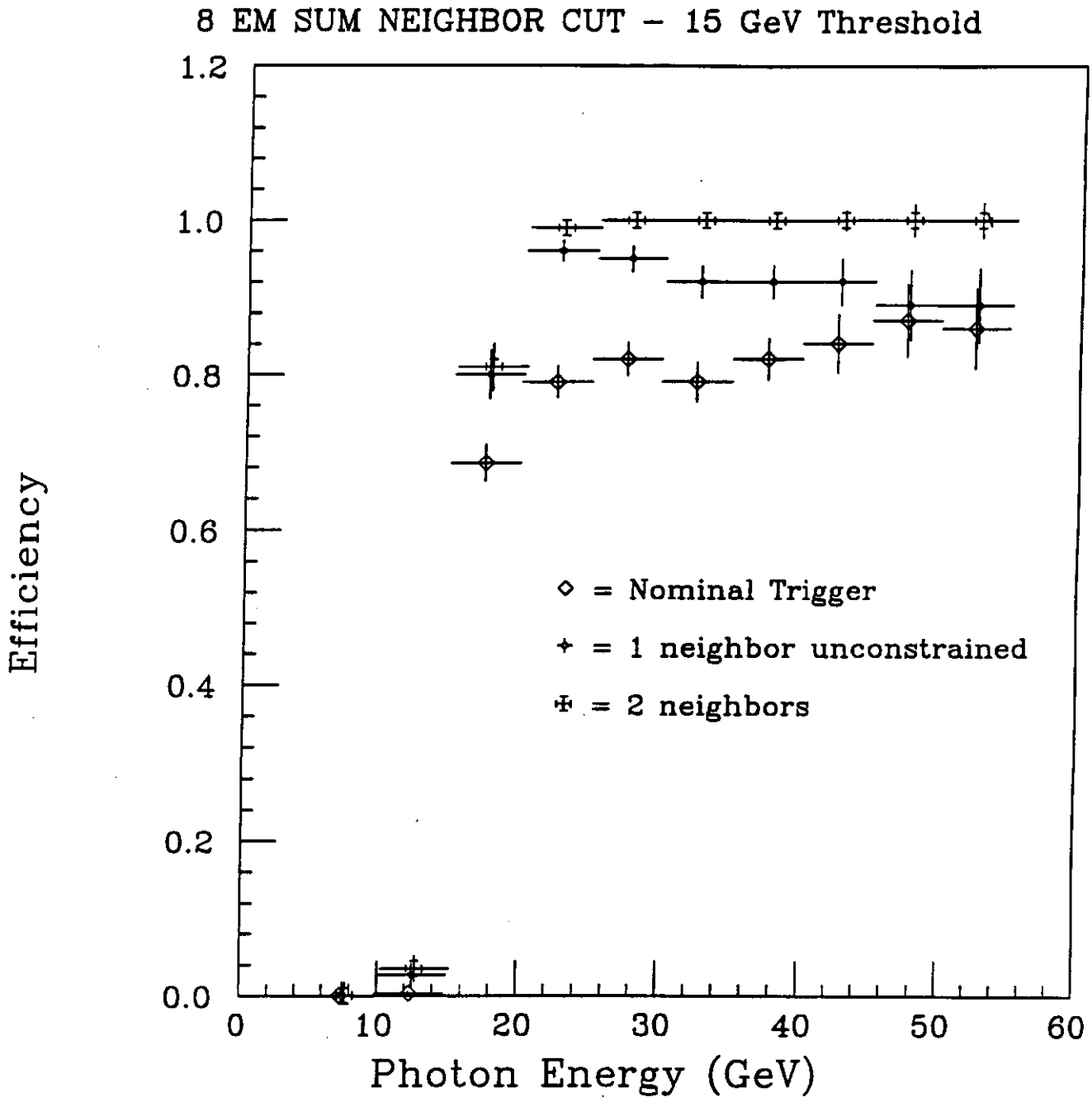

Figure 20: The trigger response as a function of photon energy, showing the photon efficiency for a trigger threshold of 15 GeV. The nominal EM-veto trigger is shown along with the curves for leaving 1 and 2 EM sums out of lateral veto for both the 2 EM sum sharing, and for the isolated EM sum parts of the single photon trigger. The plateau efficiency reaches the desired 100 % for the second case, demonstrating that lateral shower spreading for the otherwise isolated EM sum part of the trigger is responsible for the bulk of the trigger inefficiency when the photon energy is far above threshold. Interestingly enough, the efficiency for the case of 1 neighbor left unconstrained begins to follow this same curve, but again falls as the photon energy becomes large.

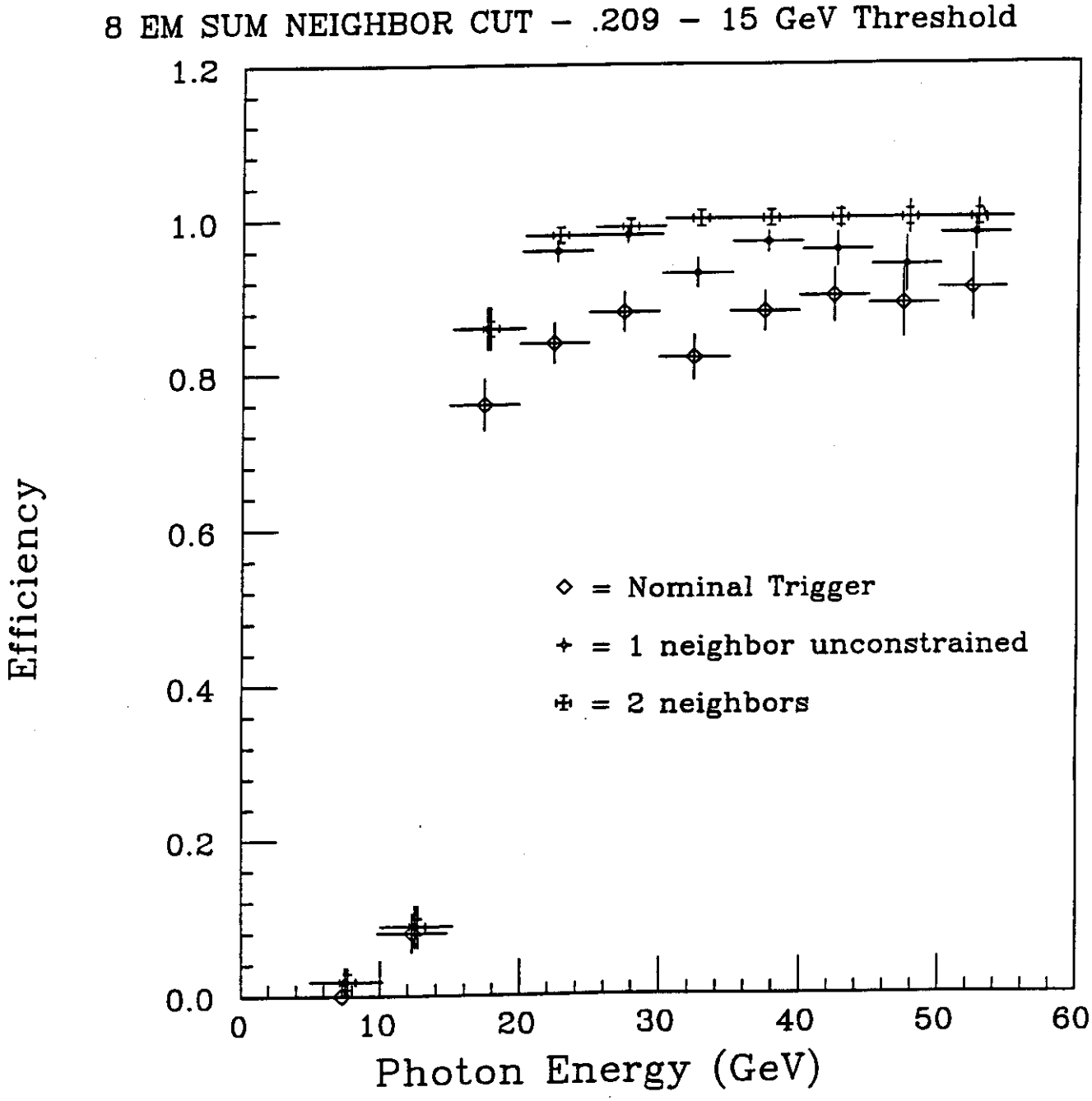

Figure 21: The trigger response as a function of photon energy, showing the photon efficiency for a trigger threshold of 15 GeV. This is the same as Figure 20, but now for the .209x.209 EM sum segmentation. The plateau efficiencies are higher, showing somewhat less lateral shower spreading, but the conclusions are the same.

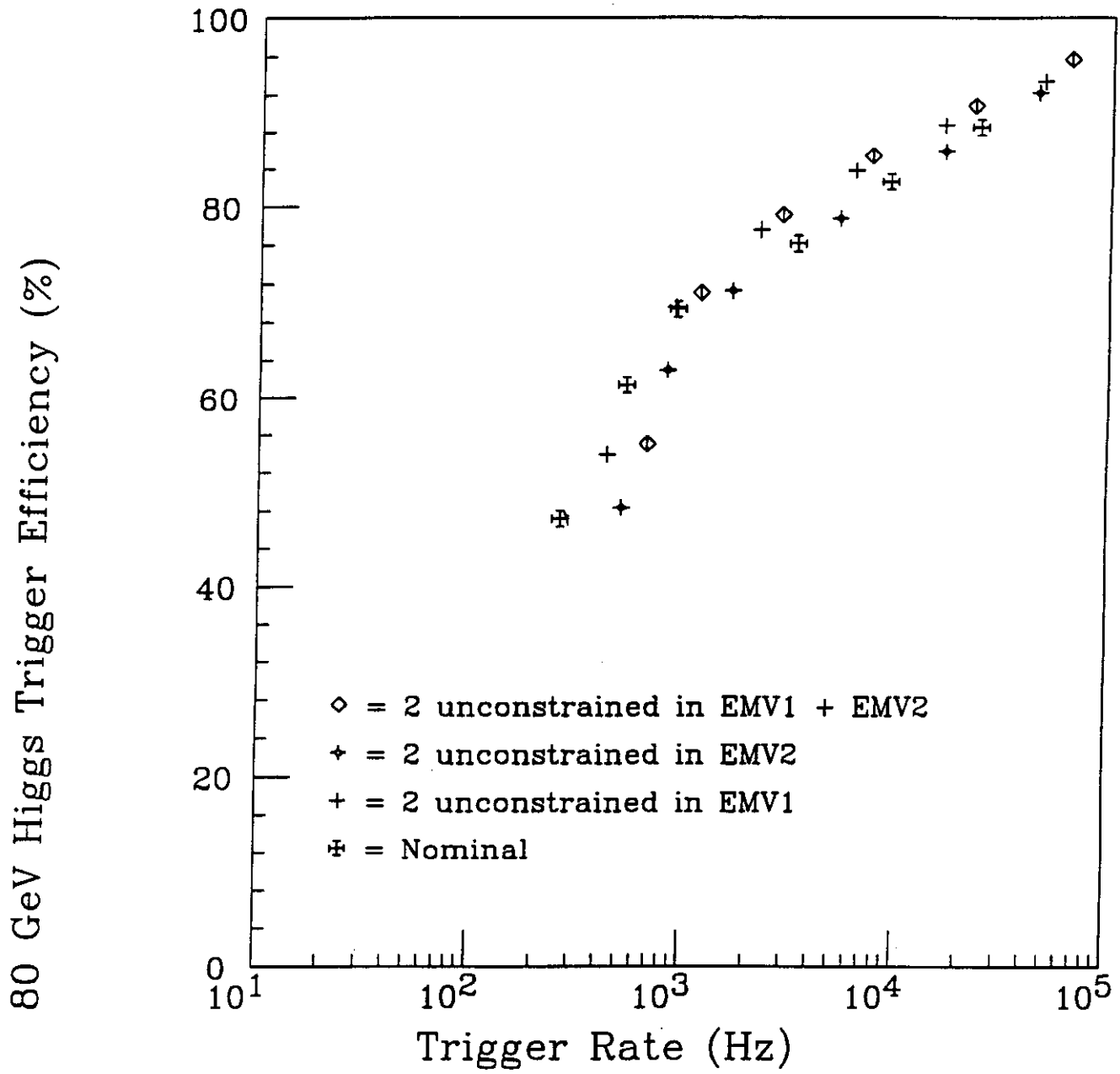

Figure 22: The Higgs Efficiency versus the background trigger rate for the nominal EM-veto trigger, and those leaving 2 neighbors unconstrained in the lateral veto. One leaves the neighbors unconstrained only the case of the 2 EM sum shower sharing (EMV2), one only in the case of the isolated EM sum trigger (EMV1), and the third leaves 2 unconstrained for both trigger conditions. The performance shows some improvement when loosening the contraint for the isolated EM sum (EMV1) trigger.

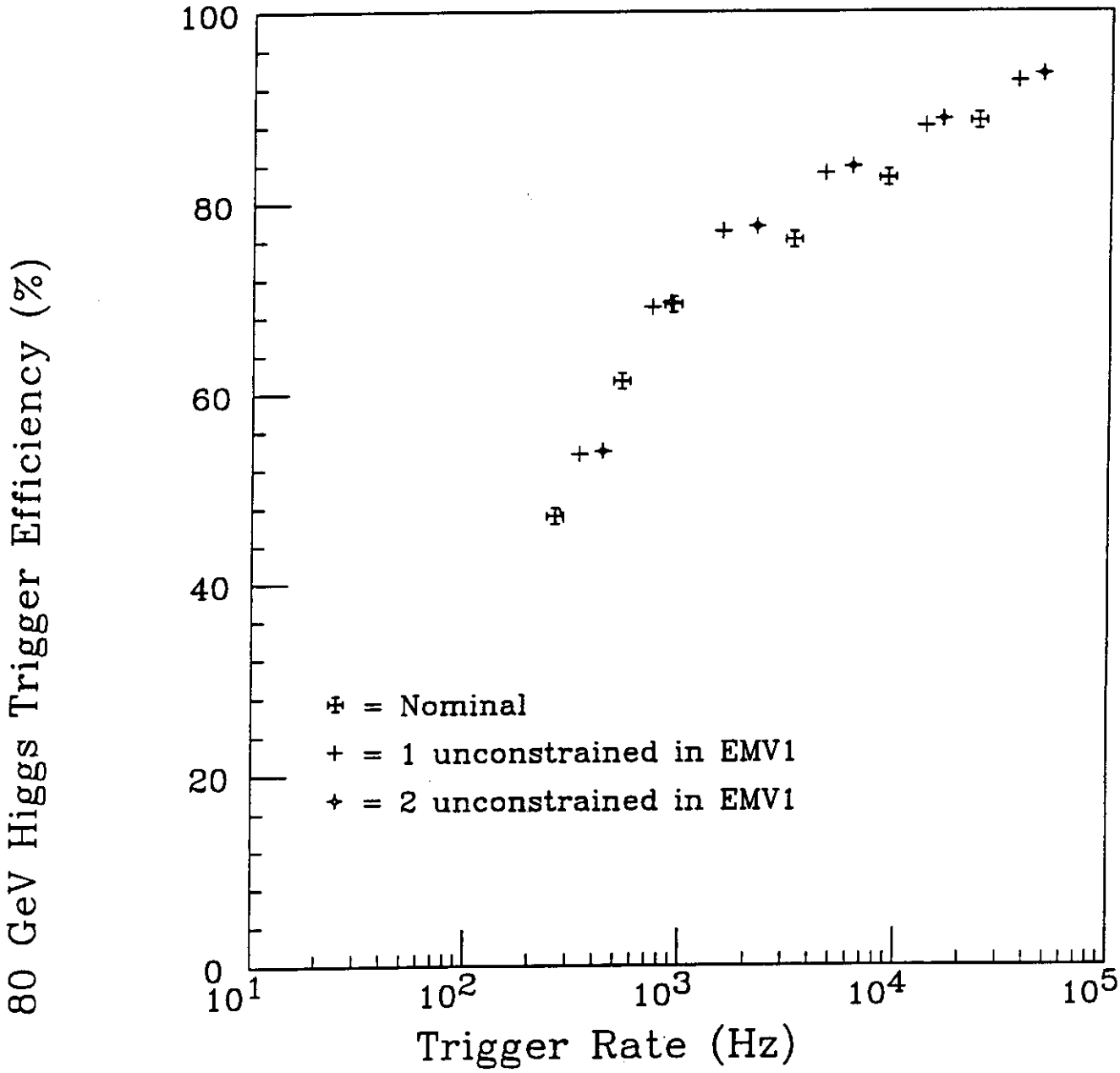

Figure 23: The Higgs Efficiency versus the background trigger rate for the nominal EM-veto trigger, and those leaving 1 and 2 neighbors unconstrained the lateral veto. These neighbors are left out of the isolated EM sum photon trigger only. The actual performance benefit comes mostly from leaving the 1 neighbor unconstrained.

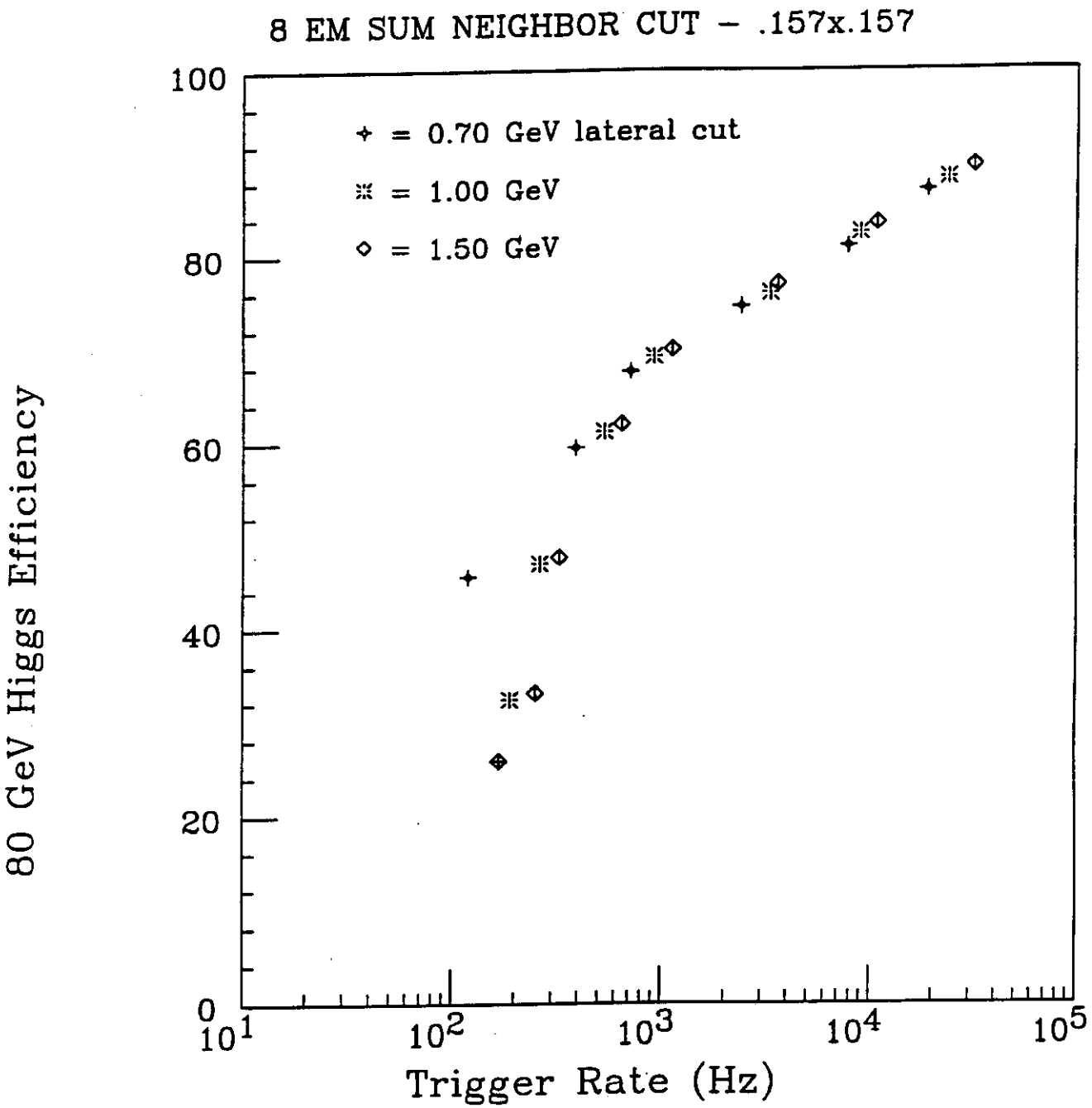

Figure 24: The Higgs Efficiency versus the background trigger rate for the nominal EM-veto trigger lateral veto cut (1 GeV), and for 2 others. There is no benefit to changing this cut.

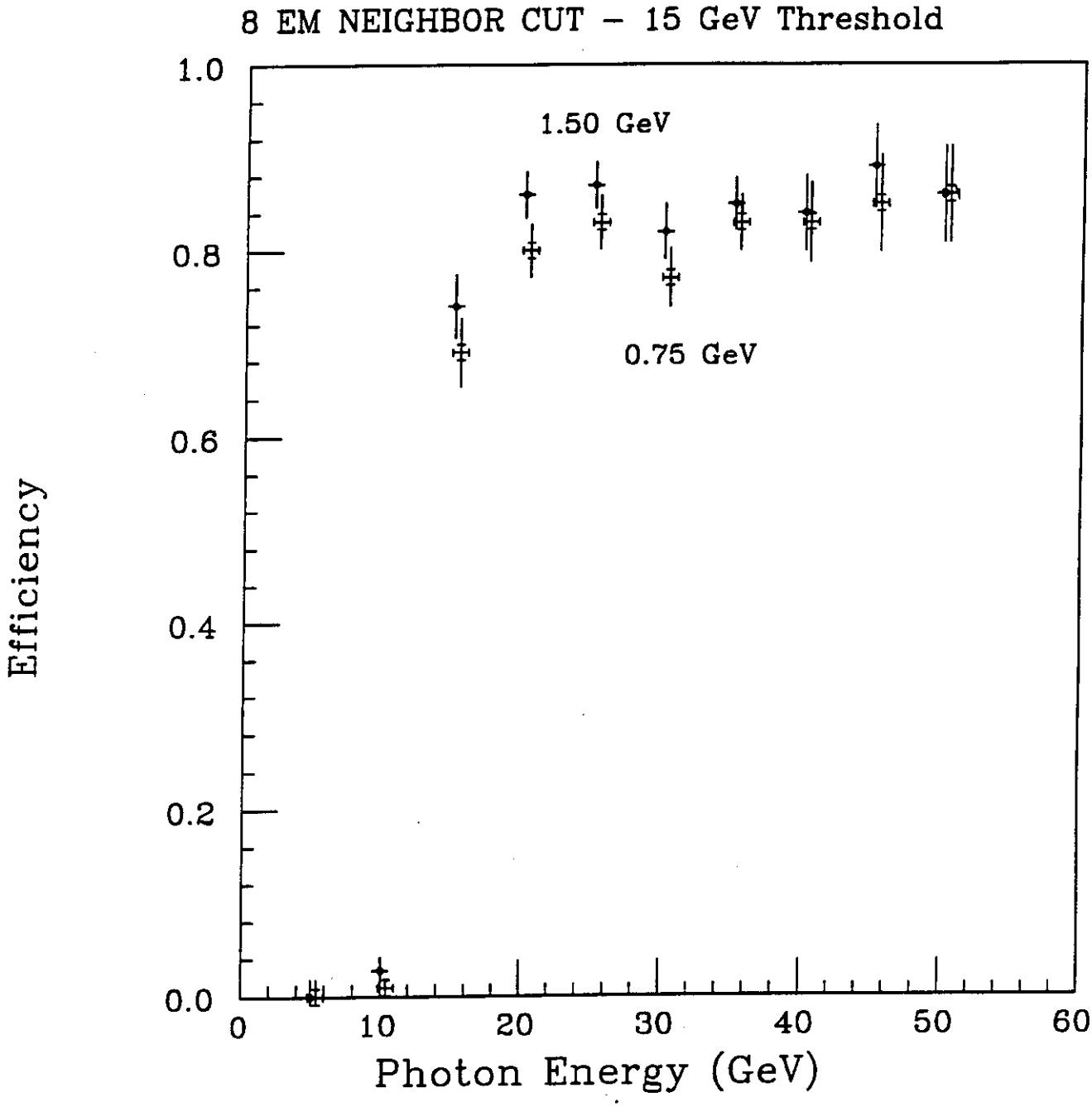

Figure 24b:The effect of changing the lateral veto level on the trigger turn-on curve is shown. There is perhaps some difference for photons near threshold, although the statistics are poor. For photons well over threshold any inefficiency from shower spreading will be insensitive to small changes in the lateral veto.

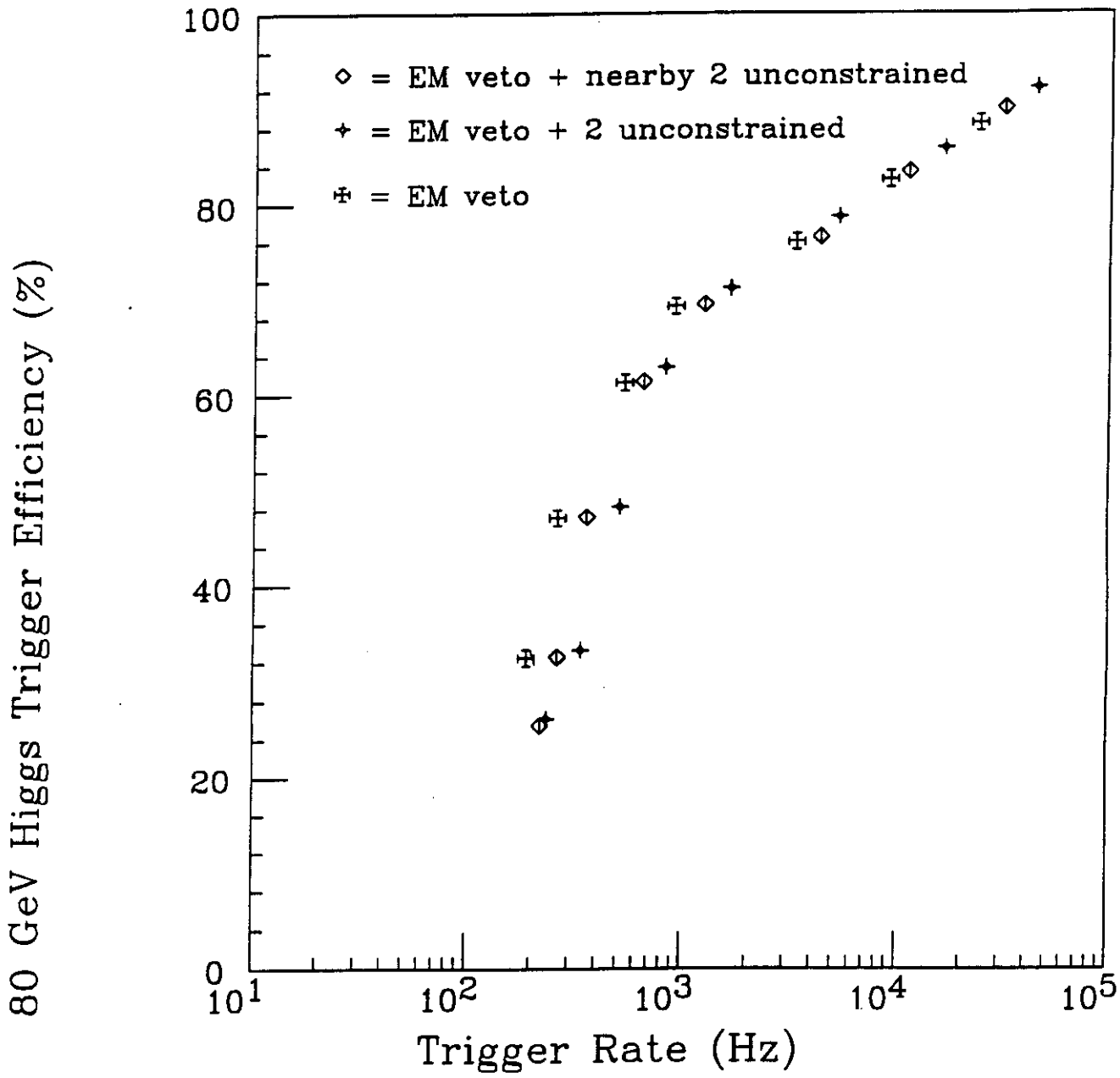

Figure 25: The Higgs Efficiency versus the background trigger rate for the nominal EM-veto trigger, and those leaving 2 neighbors unconstrained in the lateral veto. These neighbors are left out of the 2 EM sum sharing part of the photon trigger only. The points labelled 'nearby 2 unconstrained' drop the lateral veto condition for the 2 EM sums nearest the shower sharing neighbor. The points labelled '2 unconstrained' drop the lateral veto condition for the 2 EM sums that are otherwise highest in energy. There is no benefit beyond the nominal EM-veto trigger from such simple pattern recognition.

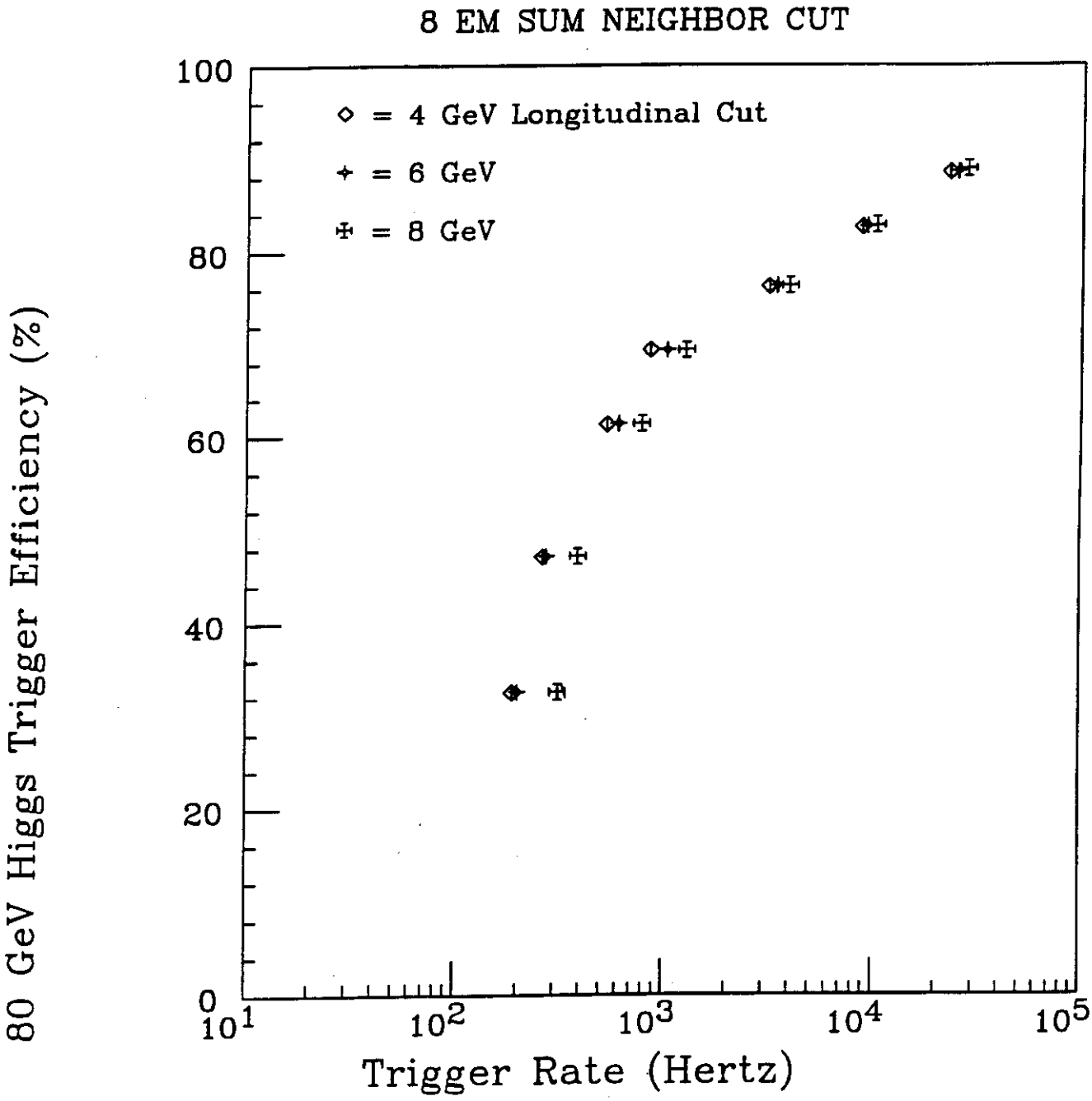

Figure 26: The Higgs Efficiency versus the background trigger rate for the nominal EM-veto trigger with 3 different hadronic veto cuts. At the highest rates, there is little benefit from this cut. The lower cut could be used for the 10**33 running, although the pileup noise would drive one to the higher cut for the 10**34 running.

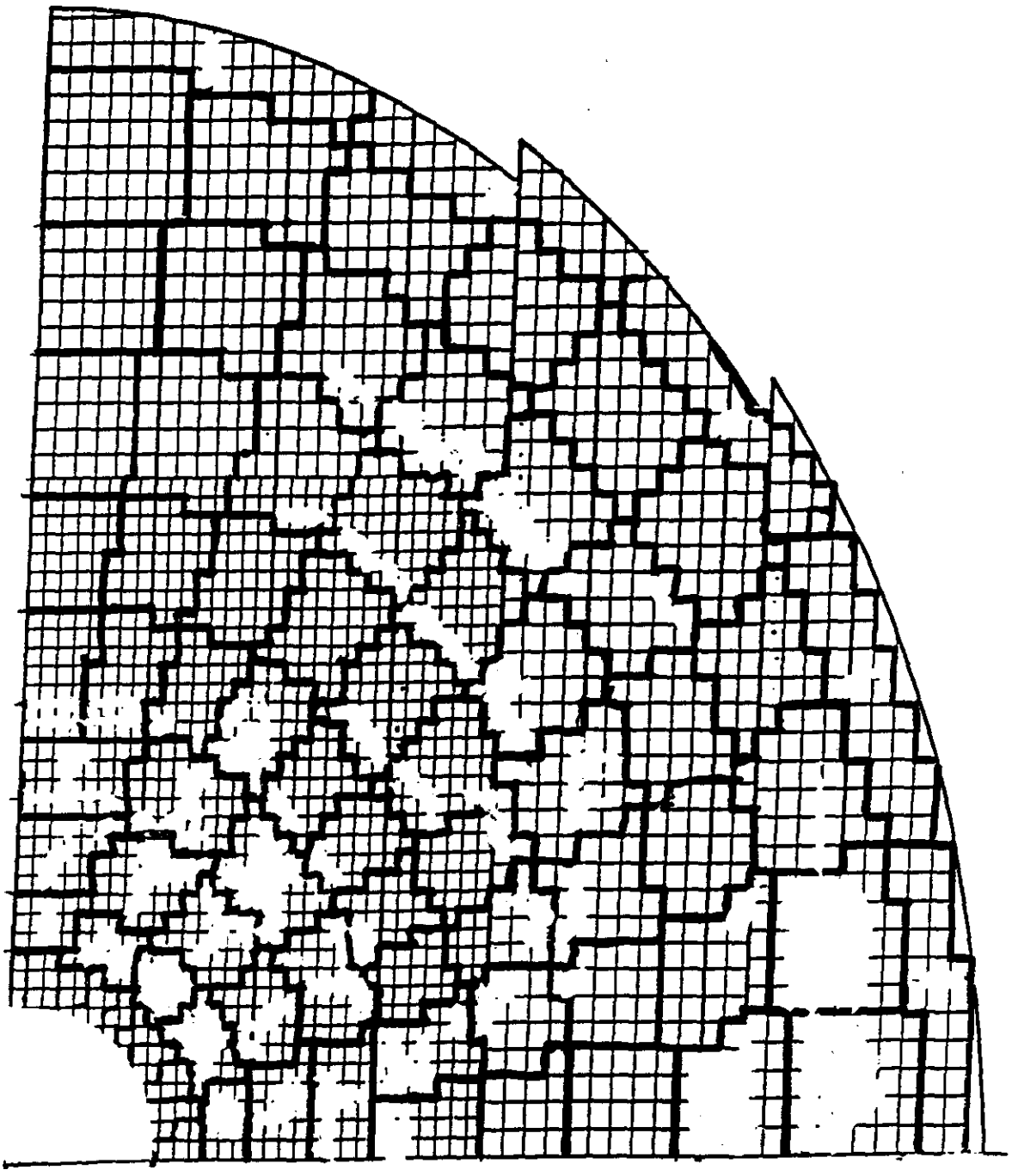

Figure 27: The proposed layout of the EM sums in the endcap calorimeter. The trigger region limit here is η=2.5. There is one row of EM sums at η higher than this limit, and one row of EM sums at the low η boundary, both for lateral veto purposes only. The actual trigger region would be from η = 1.2 to 2.5.

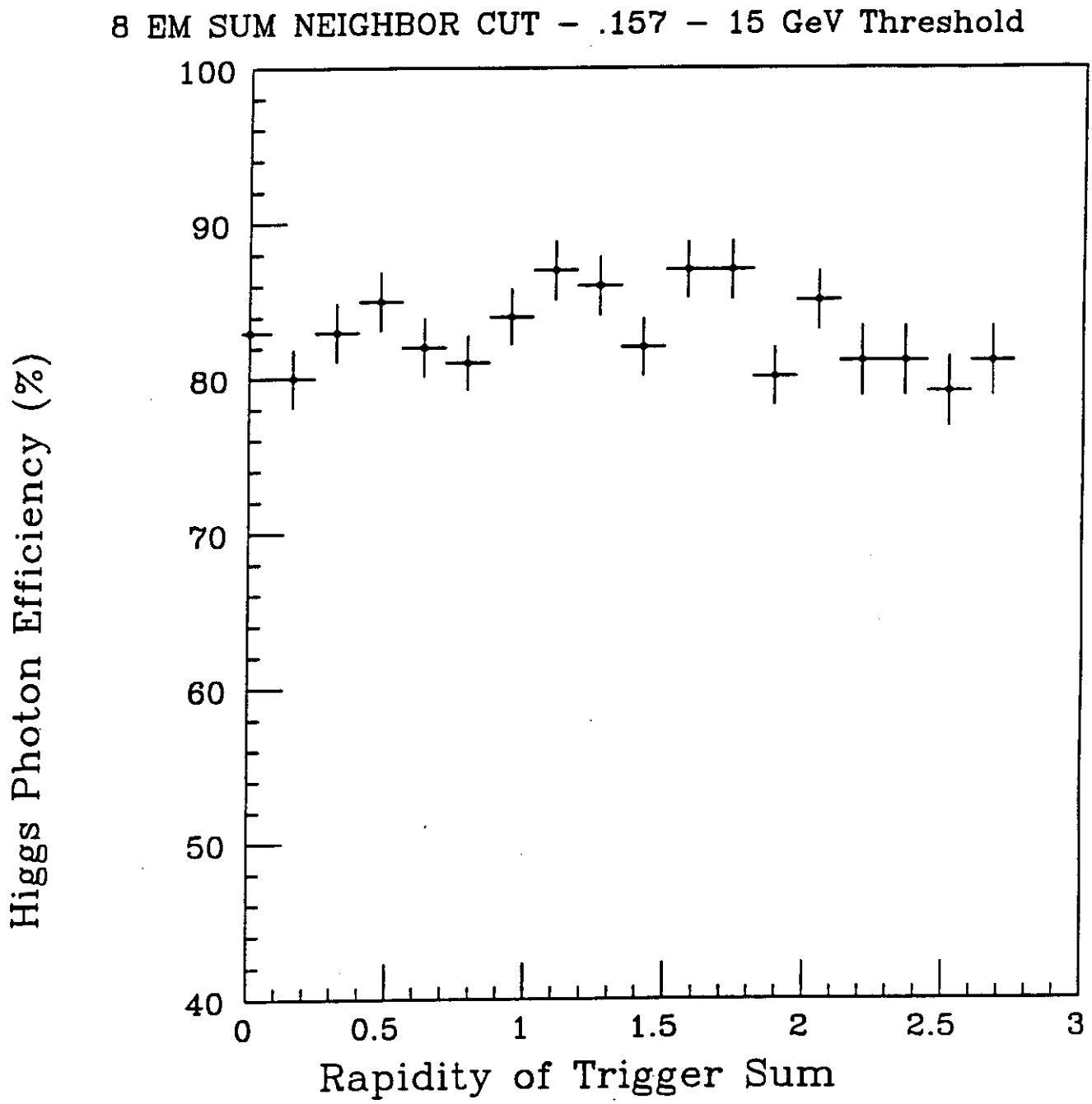

Figure 28: The Higgs Photon Efficiency versus rapidity for the nominal EM-veto trigger with a 15 GeV threshold. The efficiency is reasonably flat up to the expected trigger limit of $\eta = 2.5$.

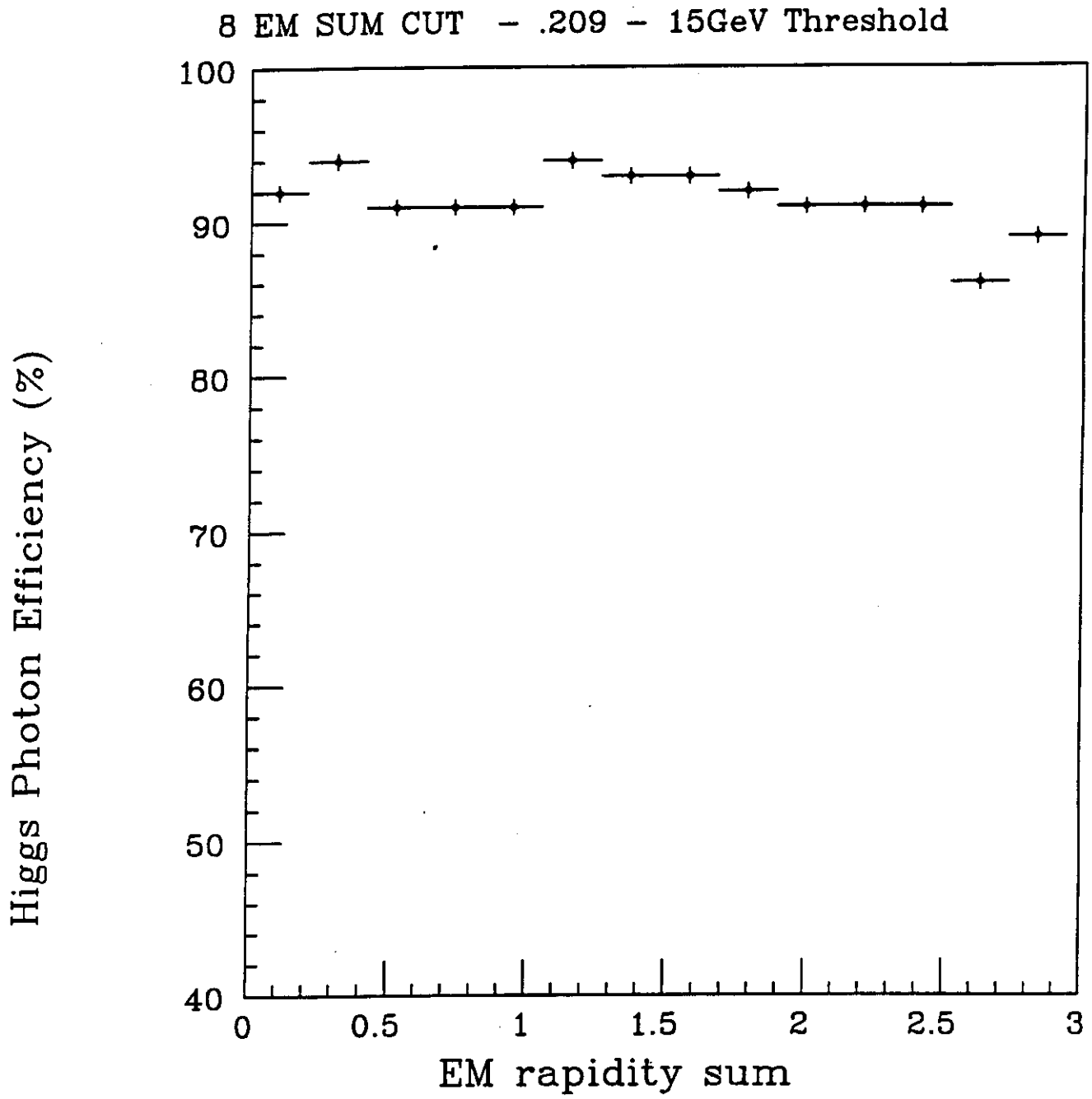

Figure 29: The Higgs Photon Efficiency versus rapidity for the nominal EM-veto trigger with a 15 GeV threshold. This is the same as Figure 28, but for an EM sum segmentation of .209x.209. The efficiency is reasonably flat up to the expected trigger limit of $\eta = 2.5$. There is an indication of a drop in efficiency outside of this limit.

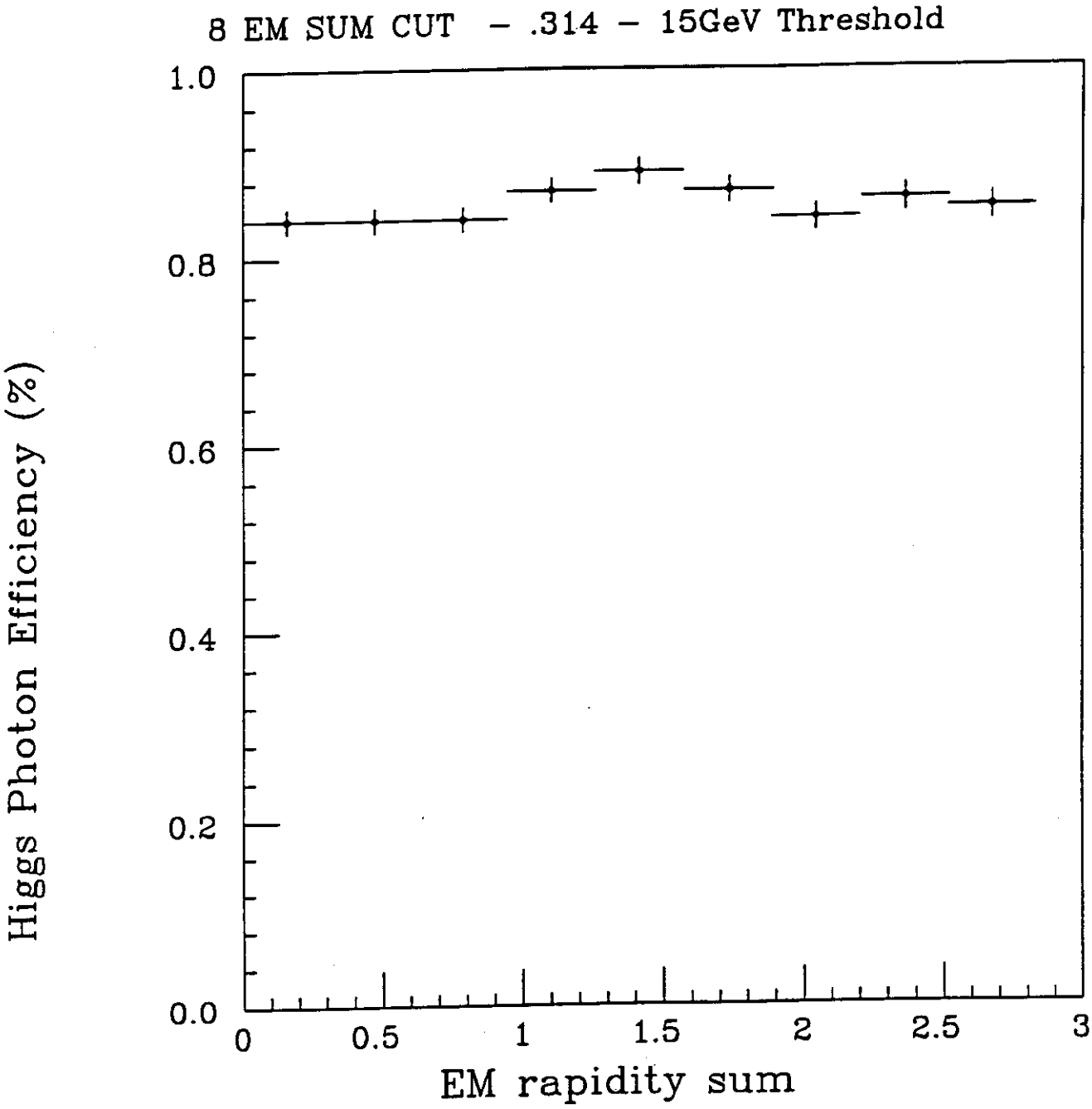

Figure 30: The Higgs Photon Efficiency versus rapidity for the nominal EM-veto trigger with a 15 GeV threshold. This is the same as Figure 28, but for an EM sum segmentation of .314x.314. The efficiency is reasonably flat up to the expected trigger limit of $\eta = 2.5$.

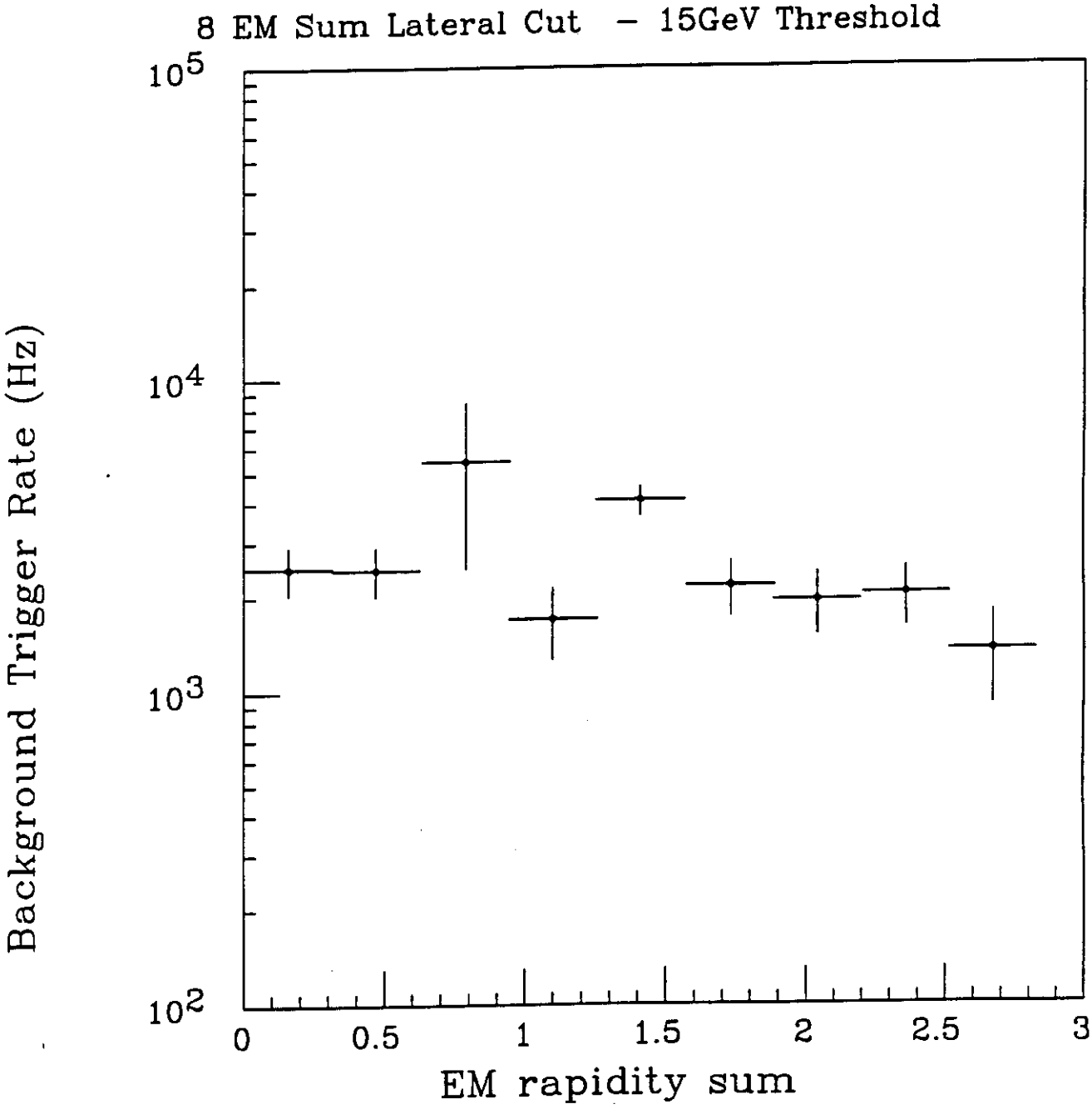

Figure 31: The background trigger rate as a function of rapidity for the EM-veto single photon trigger, at a threshold of 15 GeV. The background triggers seem flat with rapidity, within statistics, up to the expected trigger limit of η=2.5.

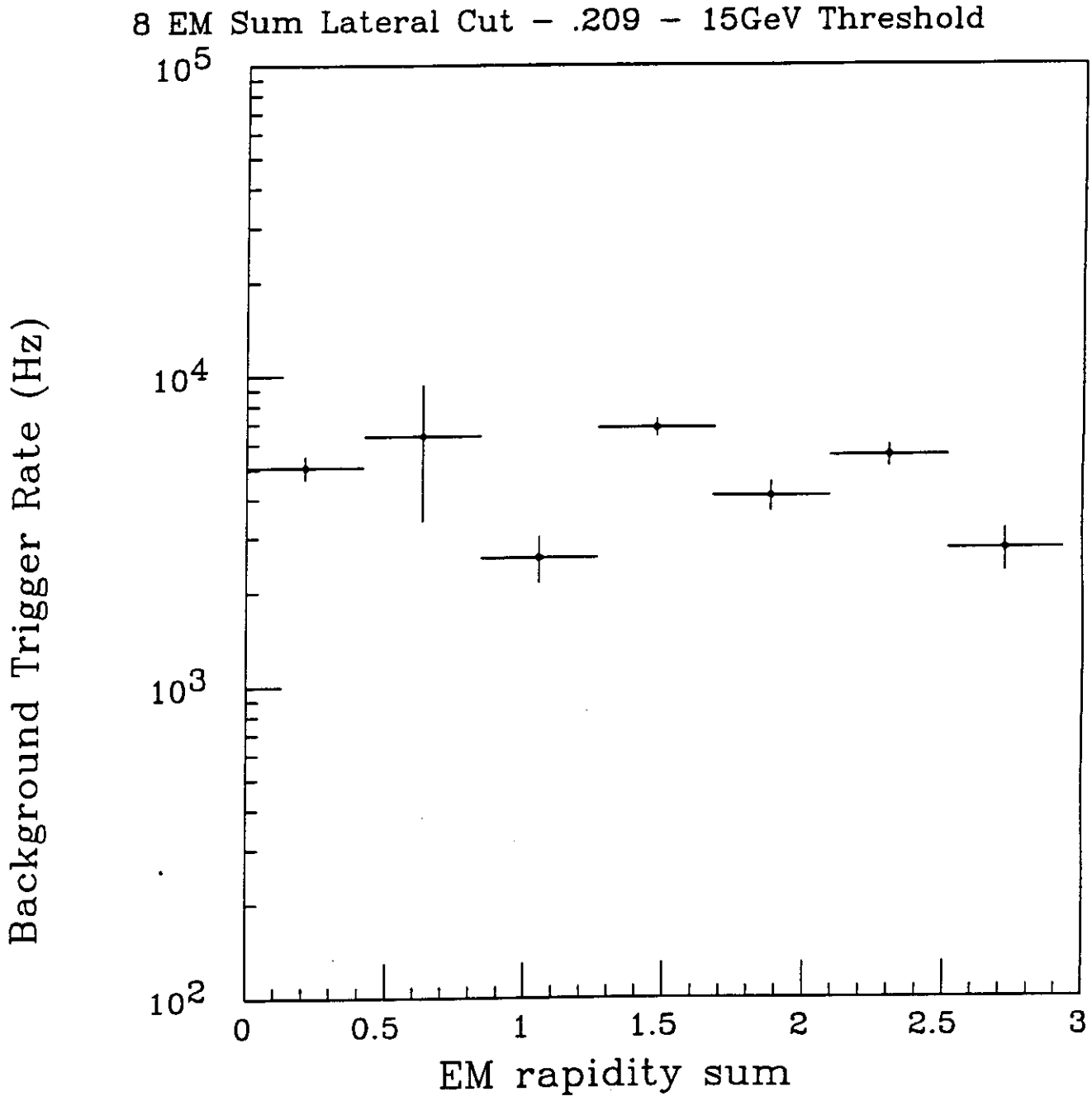

Figure 32: The background trigger rate as a function of rapidity for the EM-veto single photon trigger, at a threshold of 15 GeV. This is the same as Figure 31, except that the EM sum segmentation is .209x.209. The background triggers seem flat with rapidity, within statistics, up to the expected trigger limit of η=2.5.

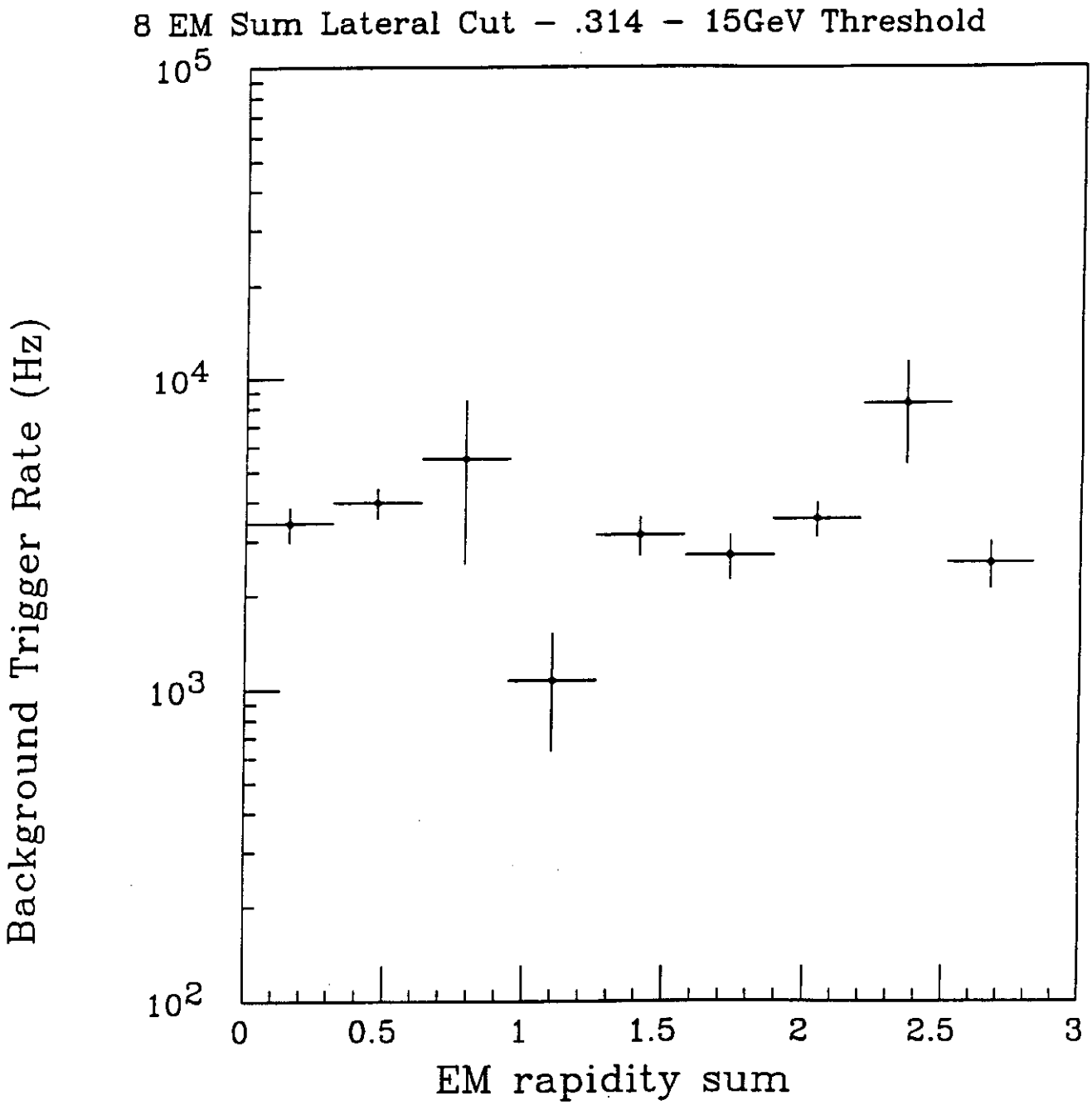

Figure 33: The background trigger rate as a function of rapidity for the EM-veto single photon trigger, at a threshold of 15 GeV. This is the same as Figure 31, except that the EM sum segmentation is .314x.314. The background triggers seem flat with rapidity, within statistics, up to the expected trigger limit of η=2.5. There is no gap between the barrel region and the endcap region, as might seem to be indicated.

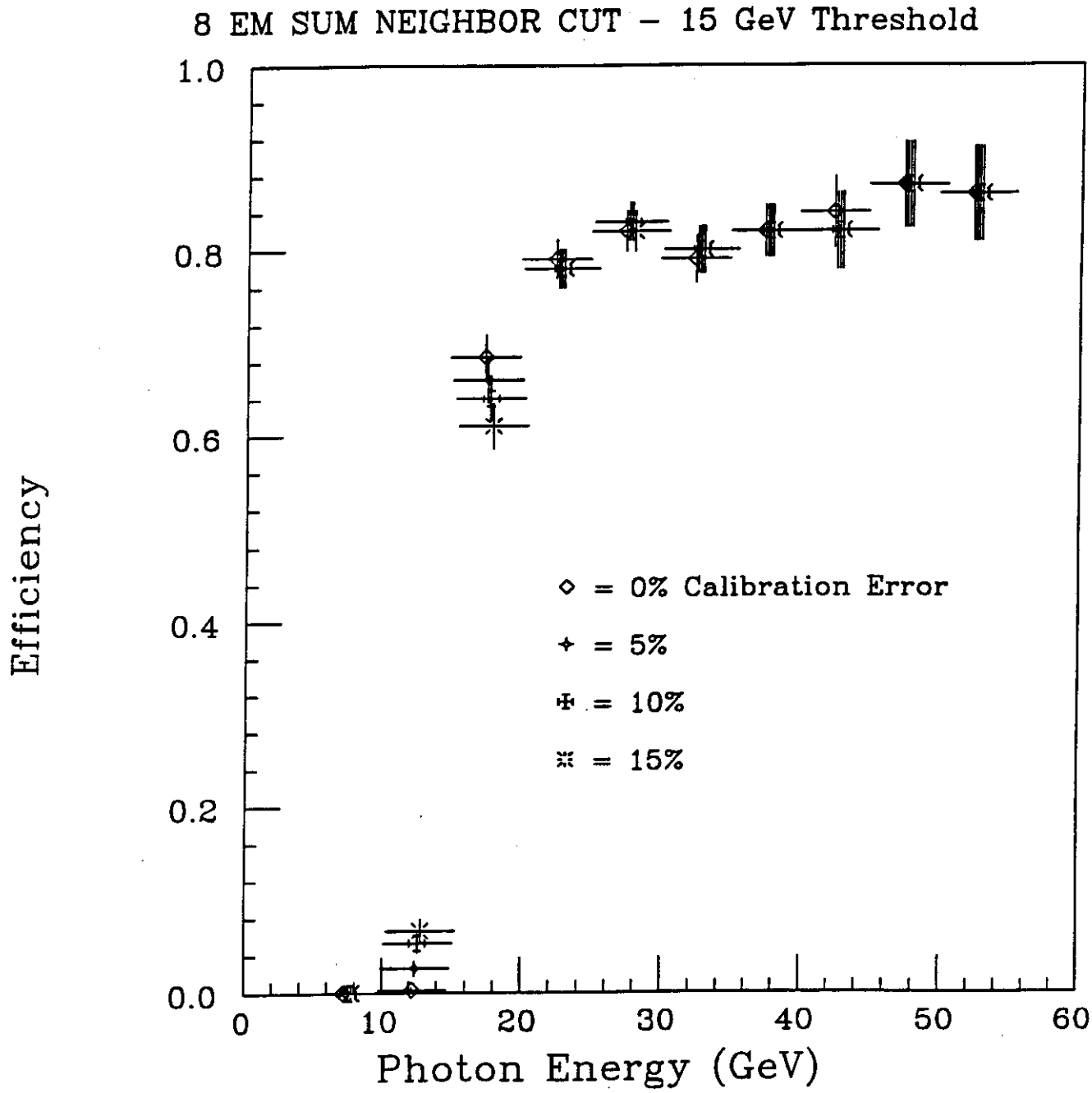

Figure 34: The trigger response as a function of photon energy, showing the photon efficiency for a trigger threshold of 15 GeV. The nominal EM-veto trigger is shown along with the curves 5%, 10% and 15% intercalibration error between EM towers. The edge at the threshold is degraded as the calibration error goes up, but not the plateau region. Considering the shower sharing problems already discussed at threshold, calibration errors are not expected to be a problem.

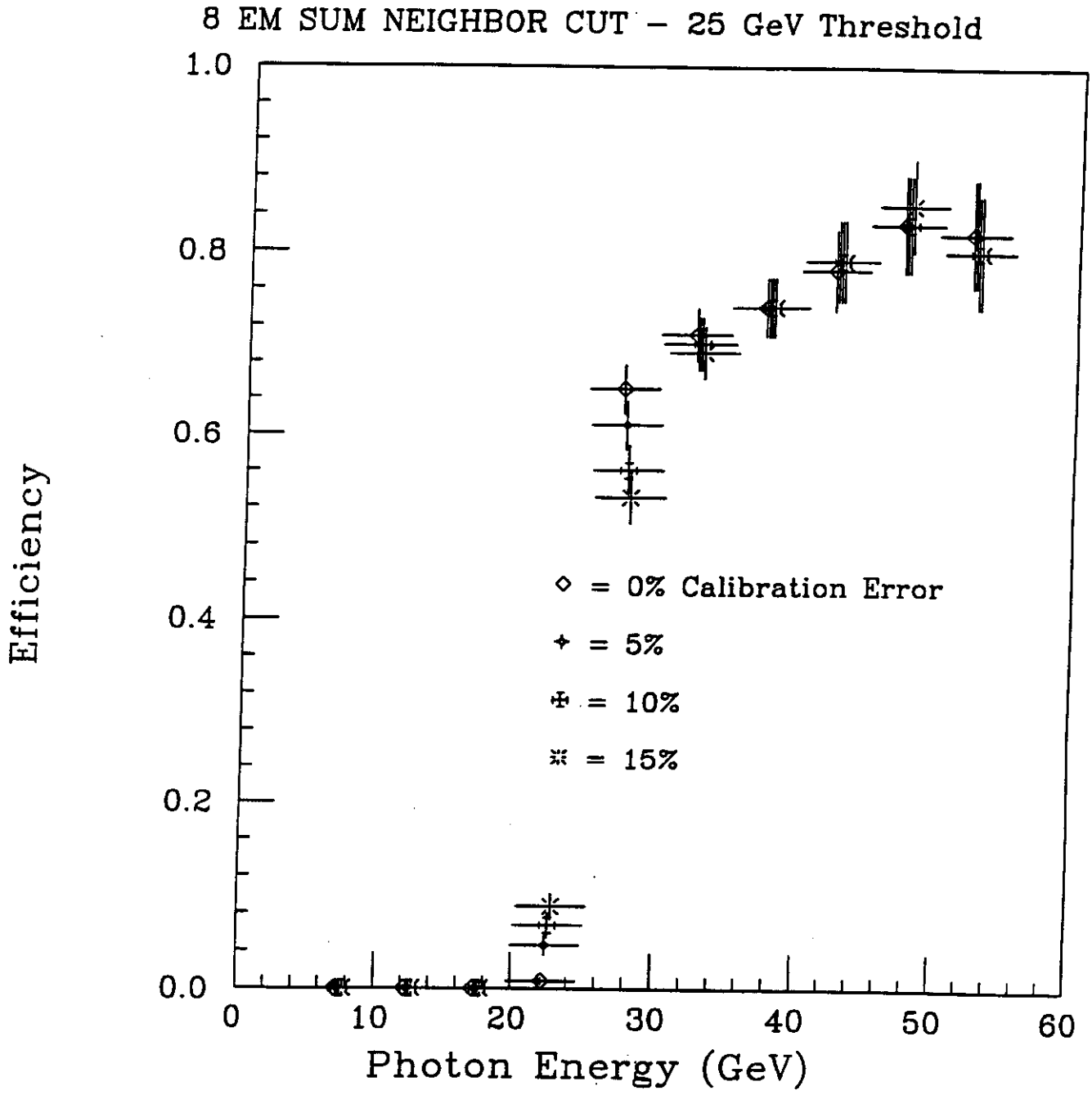

Figure 35: The trigger response as a function of photon energy, showing the photon efficiency for a trigger threshold of 25 GeV. The conclusion is much the same as in figure 34. The edge is degraded, but the shoulder and plateau are hardly affected.

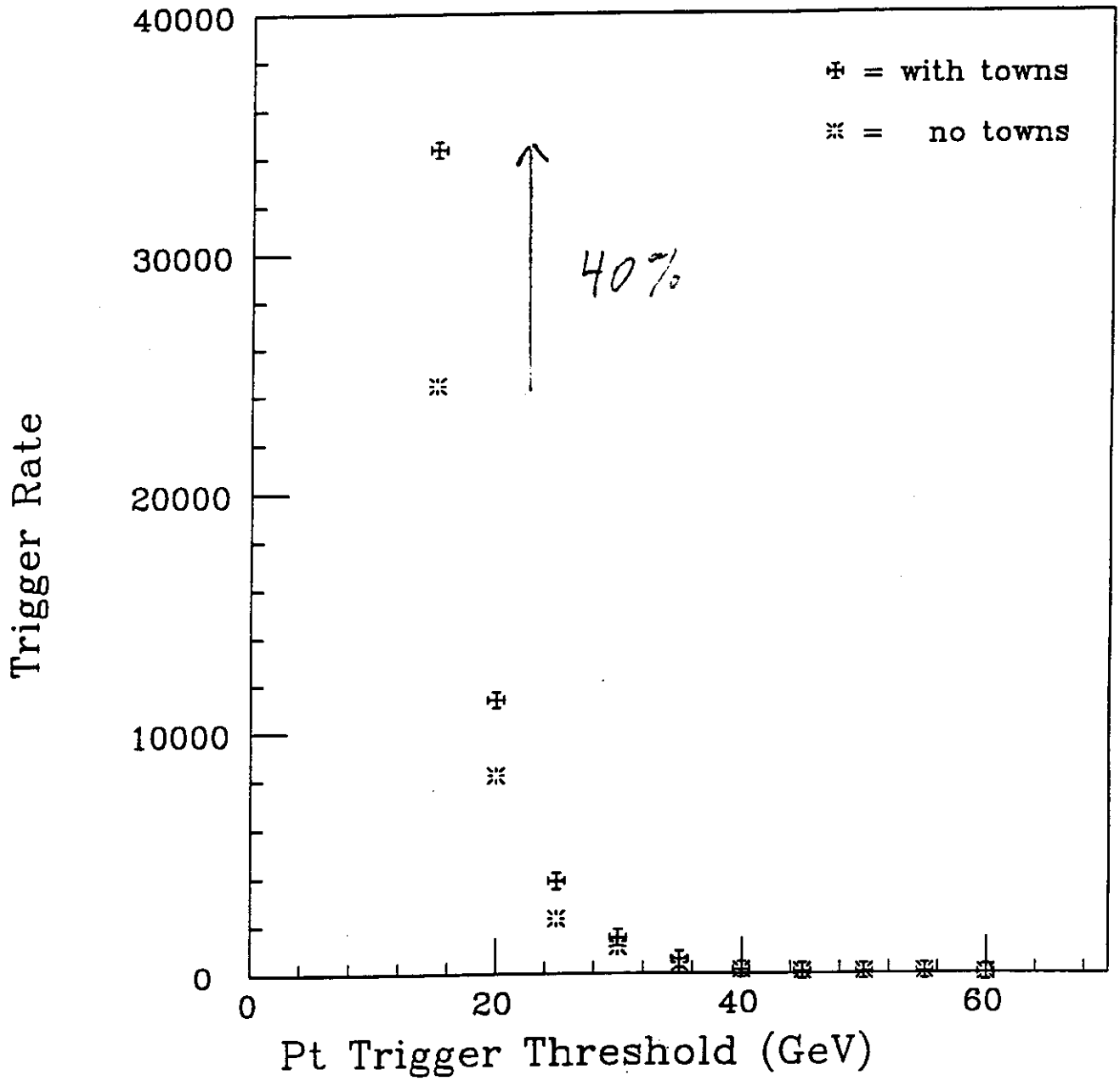

Figure 36: Comparison of background trigger rates for the baseline SP-veto single photon trigger, with and without trigger towns. By breaking up the lateral vetoing neighborhoods into towns, the trigger rate goes up by 40%.

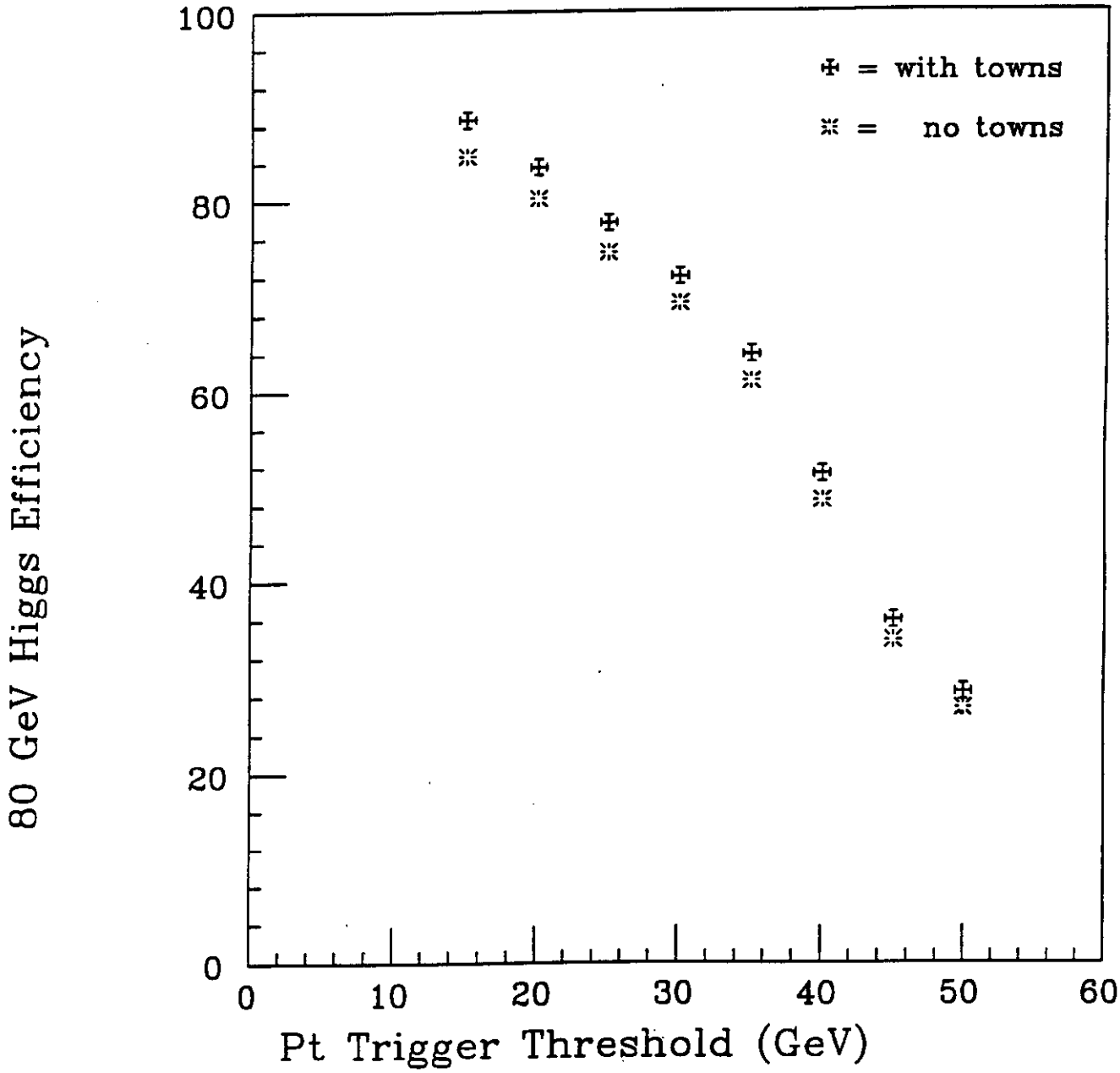

Figure 37: The Higgs Efficiency for the baseline SP-veto single photon trigger, with and without trigger towns. The efficiency shows a modest few percent rise without the towns.

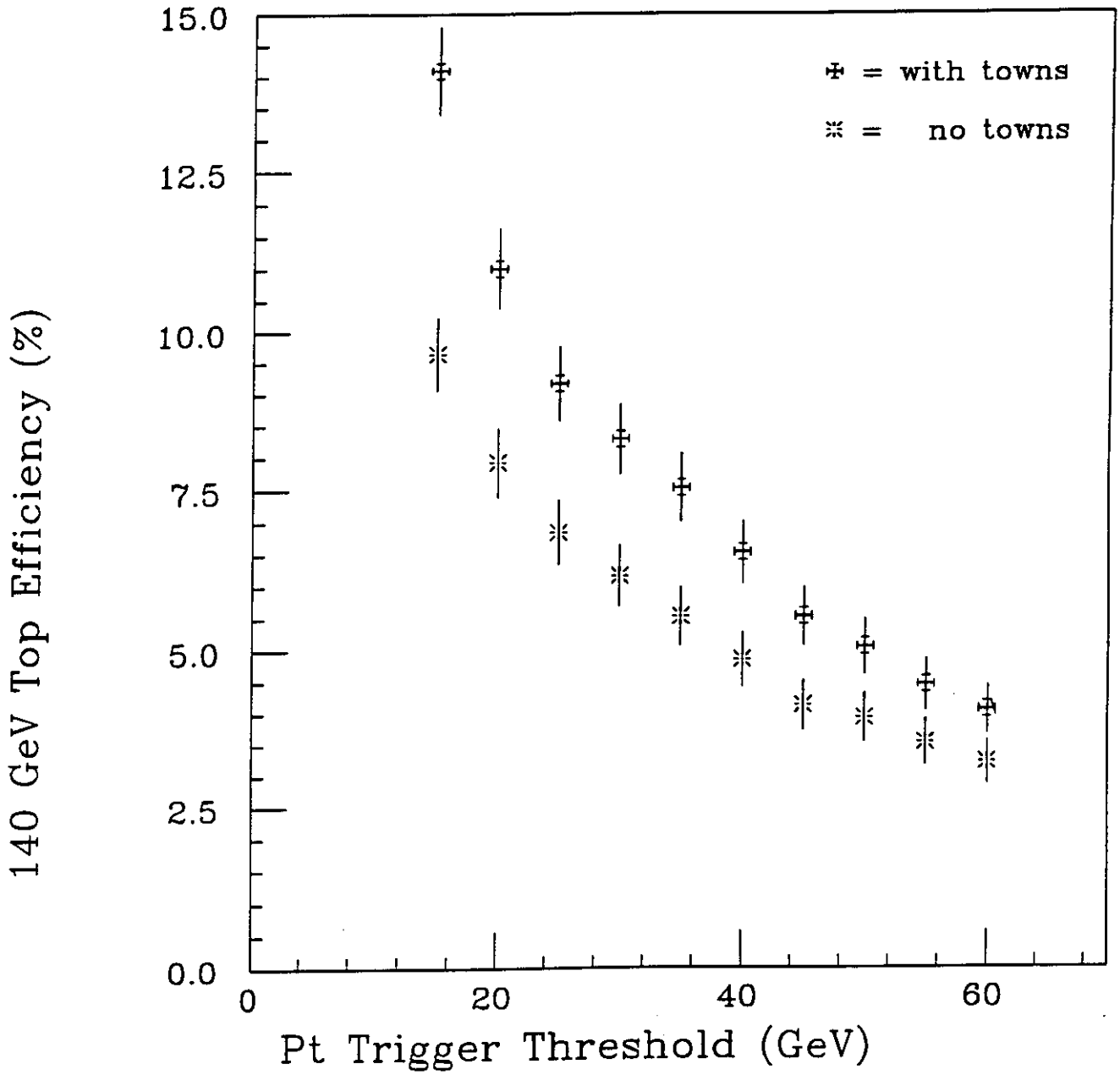

Figure 38: The top Efficiency for the baseline SP-veto single photon trigger, with and without trigger towns. The efficiency for top goes up by almost half, again showing that the top jet signal is strongly correlated with its own nearby calorimeter energy deposits.

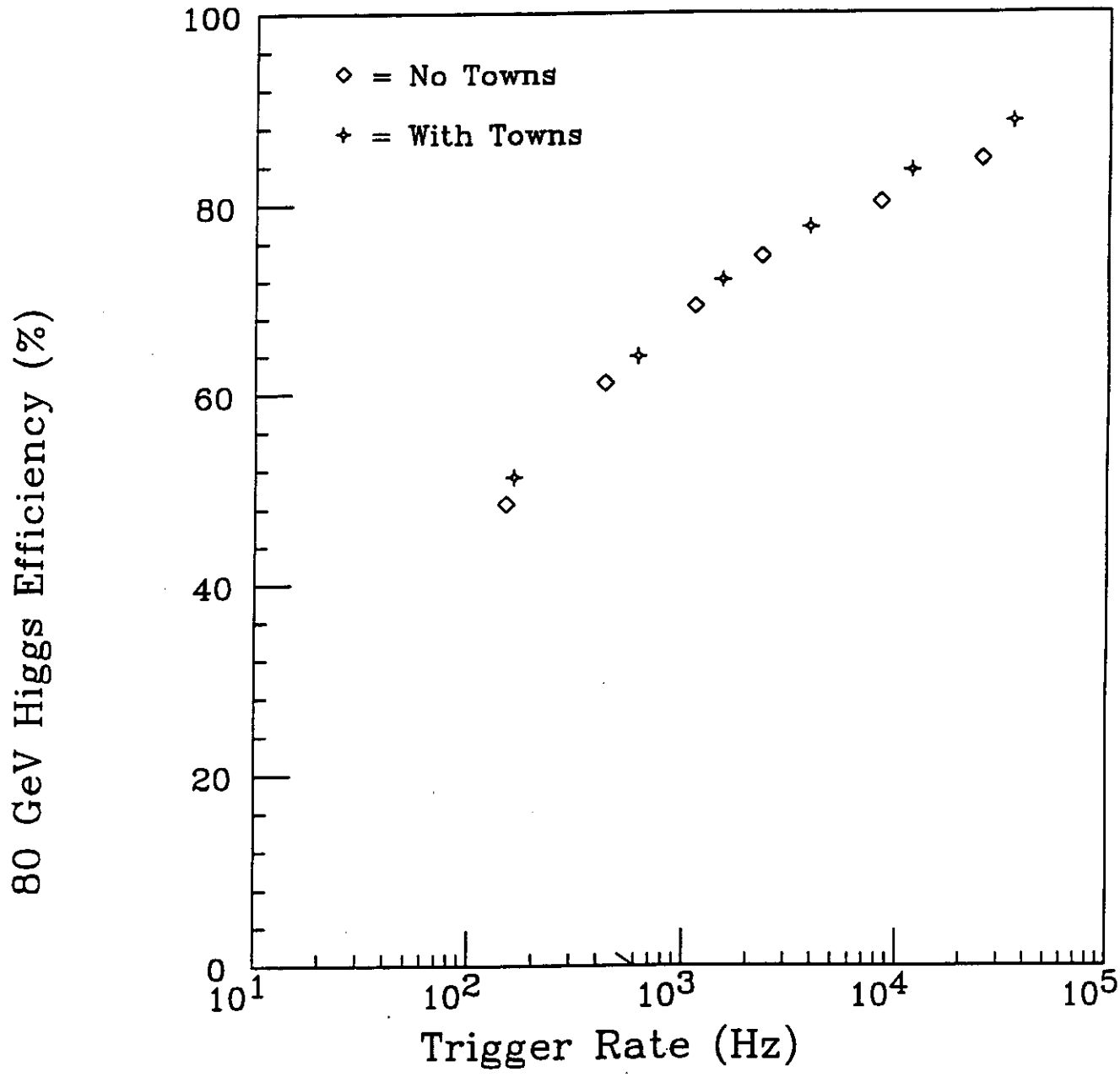

Figure 39: The Higgs efficiency versus the background trigger rate for the baseline SP-veto single photon trigger. The performance of the trigger for Higgs is unchanged by the breaking up of the lateral veto neighborhoods into trigger towns.

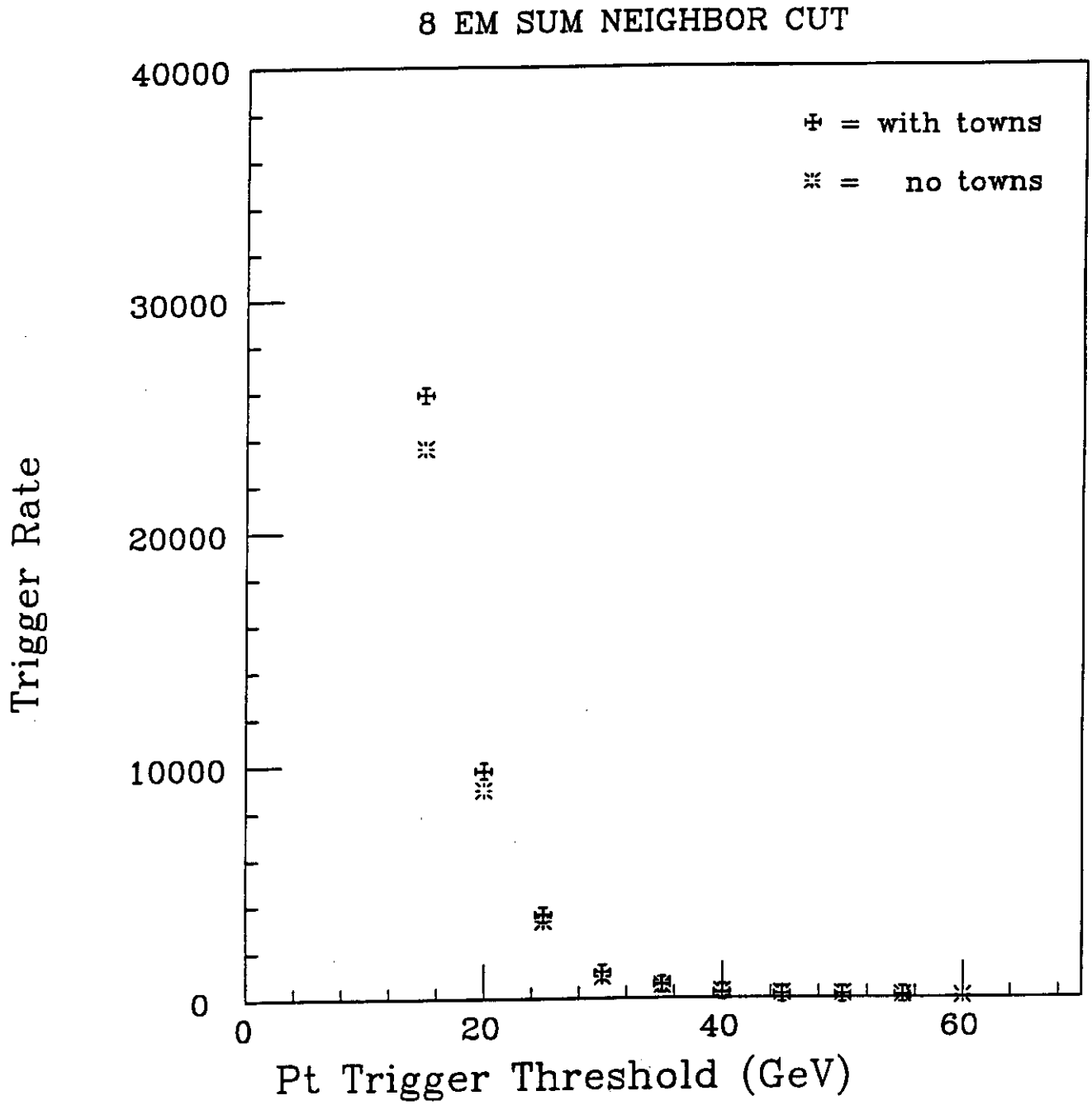

Figure 40: A comparison of background trigger rates for the EM-veto single photon trigger, with and without trigger towns. The case using the trigger towns shows a smaller increase in rate over the nominal than does the SP-veto case. Here the increase at the lowest thresholds is 13%.

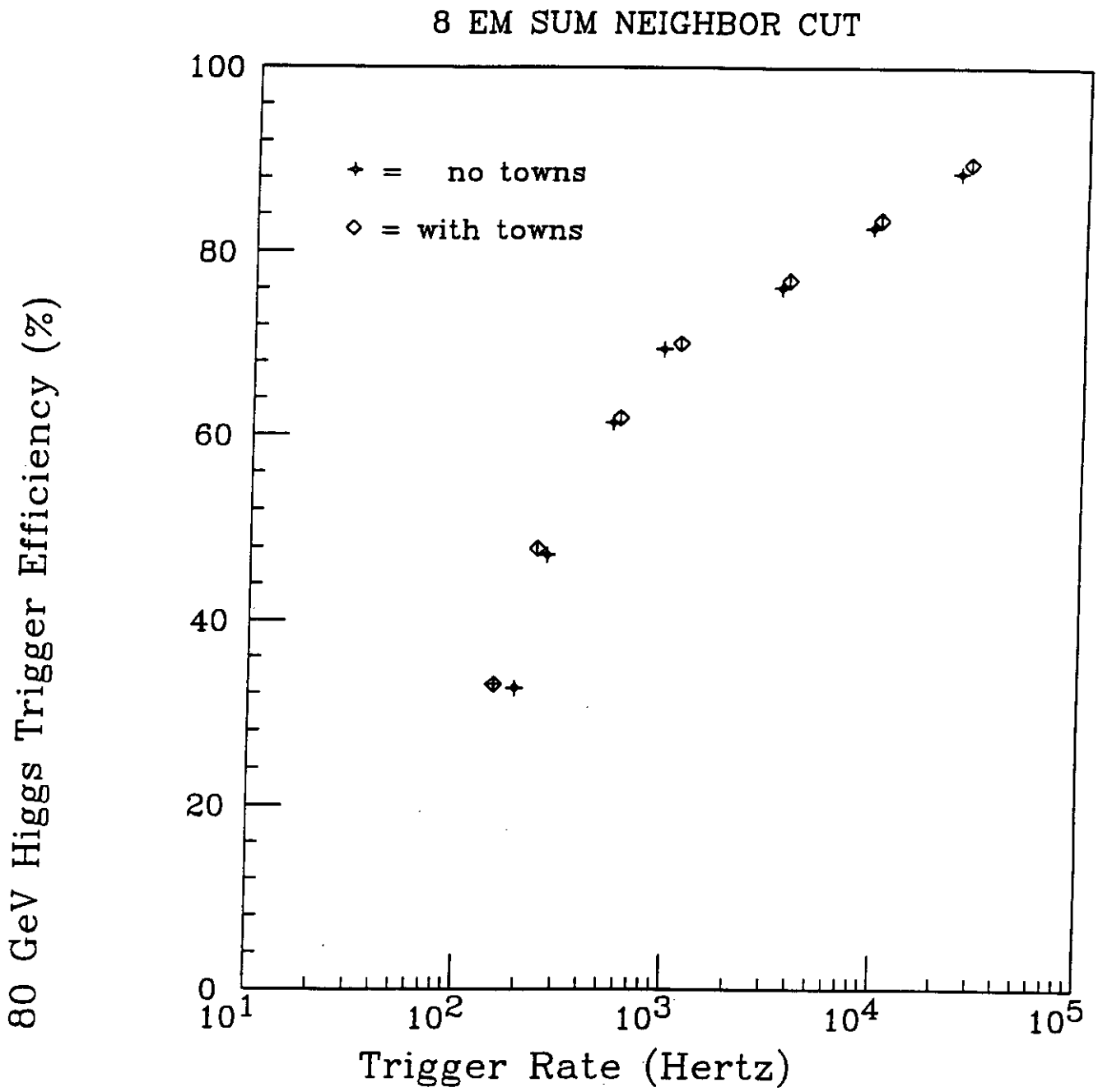

Figure 41: A comparison of Higgs efficiency versus background trigger rates for the EM-veto single photon trigger, with and without trigger towns. The actual trigger performance is changed very little with this lateral veto scheme by incorporating the trigger towns.

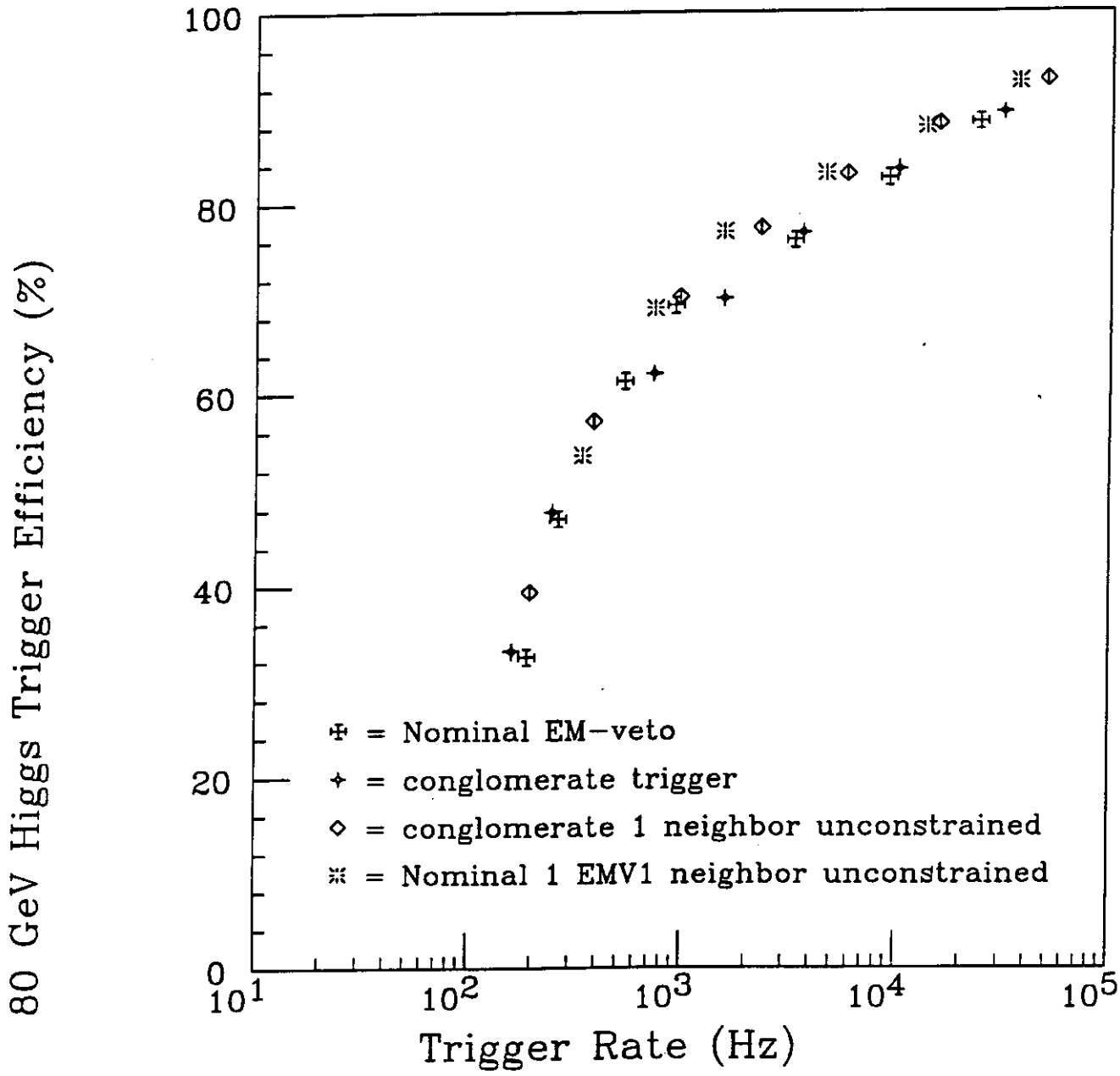

Figure 42: A comparison of Higgs efficiency versus background trigger rates for a conglomerate single photon trigger, using the EM sums for the lateral veto and the SPEM sums for the isolated shower containment. Also shown is the effect in the nominal trigger in leaving out 1 neighbor from the lateral veto, compared to this conglomerate trigger. There is little added benefit over the nominal EM lateral veto trigger.

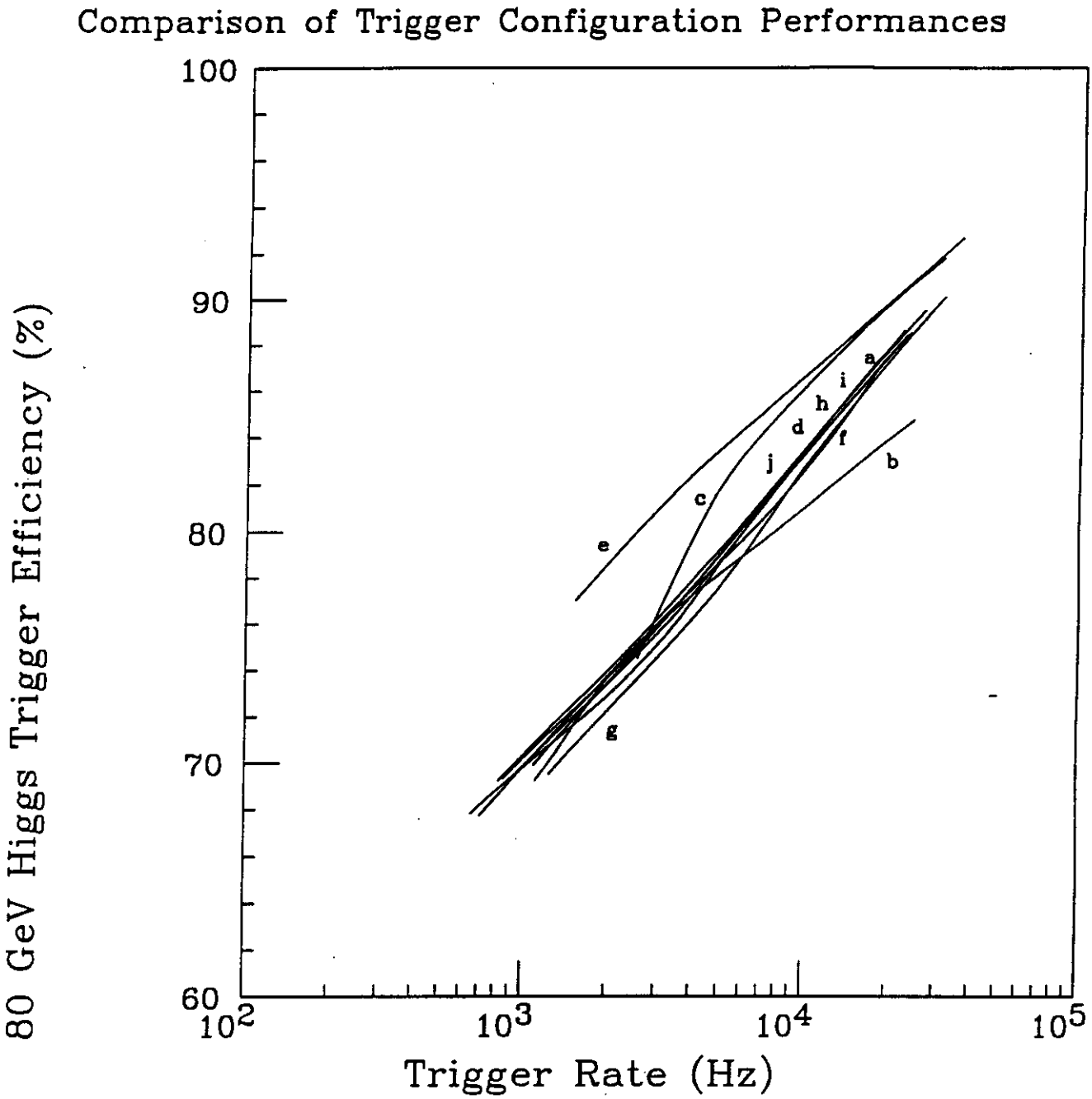

Figure 43: A comparison of Higgs efficiency versus background trigger rates for most of the trigger configurations discussed here. See Table 2 for descriptions. Most trigger performances fall on the same curve. The TDR baseline is curve "b".

Curve	Figure	Lat Veto	Had Veto	Other
a	12	EM 1 GeV	SP 5 GeV	EM sum trigger
b	6	SP 1 GeV	4 SP 5 GeV	SPEM TDR-baseline
c	12	EM 1 GeV	SP 5 GeV	.209 x .209
d	15	EM 1 GeV	SP 5 GeV	2 lateral rings
e	23	EM 1 GeV	SP 5 GeV	1 unc in EMV1
f	42	EM 1 GeV	SP 5 GeV	trigger towns
g	25	EM 1 GeV	SP 5 GeV	EMV2 pattern
h	24	EM .7 GeV	SP 5 GeV	vary cut
i	26	EM 1 GeV	SP 4 GeV	vary cut
j	9	EM 1 GeV	4 SP 5 GeV	larger had. area

Table 2: Summary of Trigger conditions varied during this study. See Figure 44. The proposed trigger now is curve "e".